Geoscientific Model Development Discussions

Open Access

SPHY v2.0: Spatial Processes in HYdrology

W. Terink[1], A. F. Lutz[1], G. W. H. Simons[1,3], W. W. Immerzeel[1,2], and P. Droogers[1]

[1]FutureWater, Costerweg 1V, 6702 AA Wageningen, the Netherlands
[2]Utrecht University, Department of Physical Geography, Heidelberglaan 2, 3508 TC Utrecht, the Netherlands
[3]Delft University of Technology, Faculty of Civil Engineering and Geosciences, Department of Watermanagement, Stevinweg 1, 2628 CN Delft, the Netherlands

Discussion Paper | Discussion Paper | Discussion Paper | Discussion Paper |

GMDD

8, 1687–1748, 2015

SPHY v2.0: Spatial Processes in HYdrology

W. Terink et al.

Title Page

Abstract | Introduction

Conclusions | References

Tables | Figures

⏮ | ⏭

◀ | ▶

Back | Close

Full Screen / Esc

Printer-friendly Version

Interactive Discussion

Abstract

This paper introduces and presents the Spatial Processes in HYdrology (SPHY) model (v2.0), its development background, its underlying concepts, and some typical applications. The SPHY model is developed using the best components of existing and well-tested simulation models, and is developed with the explicit aim to simulate terrestrial hydrology at flexible scales, under various land use and climate conditions. SPHY is a spatially distributed leaky bucket type of model, and is applied on a cell-by-cell basis. The model is written in the Python programming language using the PCRaster dynamic modelling framework. Compared to other hydrological models, that typically focus on the simulation of streamflow only, the SPHY model has several advantages: it (i) integrates most relevant hydrological processes, (ii) is setup modular, (iii) is easy adjustable and applicable, (iii) can easily be linked to remote sensing data, and (iv) can be applied for operational as well as strategic decision support. The most relevant hydrological processes that are integrated in the SPHY model are rainfall–runoff processes, cryosphere processes, evapotranspiration processes, the simulation of dynamic vegetational cover, lake/reservoir outflow, and the simulation of rootzone moisture contents. Studies in which the SPHY model was successfully applied and tested are described in this paper, and range from (i) real-time soil moisture predictions to support irrigation management in lowland areas, to (ii) detailed climate change impact studies in snow and glacier-fed river basins, to (iii) operational flow forecasting in mountainous catchments.

1 Introduction

The number and diversity of water-related challenges are large and are expected to increase in the future. Even today, the ideal condition of having the appropriate amount of good-quality water at the desired place and time, is most often not satisfied (Biswas and Tortajada, 2010; Droogers and Bouma, 2014). It is likely that climate variability

and change will intensify food insecurity by water shortages (Wheeler and von Braun, 2013), and loss of access to drinking water (Rockström et al., 2012). Current and future water related challenges are location and time specific and can vary from impact of glacier dynamics (Immerzeel et al., 2011), economic and population growth (Droogers et al., 2012), floods or extended and more prolonged droughts (Dai, 2011), amongst others.

In response to these challenges hydrologists and water resources specialists are developing modeling tools to analyze, understand and explore solutions to support decision makers and operational water managers. Despite difficulties to connect the scientific advances in hydrological modeling with the needs of decision makers and water managers, progress has been made and there is no doubt that modeling tools are indispensable in what is called good "water governance" (Droogers and Bouma, 2014; Liu et al., 2008).

The strength of models is that they can provide output on ultimate high temporal and spatial resolutions, and for difficult to observe sub-processes (Bastiaanssen et al., 2007). The most important aspect of applying models, is in their use to explore different scenarios, expressing for example, possible effects of changes in population and climate on the water cycle (Droogers and Aerts, 2005). Such scenarios are often referred to as projections. Models are also applied at the operational level to explore interventions (management scenarios) to be used by water managers and policy makers. Examples of this are changes in reservoir operation rules, water allocation between sectors, investment in infrastructure such as water treatment or desalination plants, and agricultural and irrigation practices. In other words: models enable hydrologists and water managers to change focus from a re-active towards a pro-active approach.

The number of existing hydrological models is probably in the tens of thousands (Droogers and Bouma, 2014). Some existing model-overviews cover a substantial amount of models: IRRISOFT (Irrisoft, 2014): 114, USGS (USGS, 2014): 110, EPA (EPA, 2014): 211, USACE (HEC, 2014): 18. Interesting is that in groundwater modelling ModFlow (Harbaugh et al., 2000) is the de-facto standard tool to use. For hydrological

models such a standard is lacking, although the SWAT model is increasingly becoming popular (Neitsch et al., 2009).

Traditionally, hydrologists have put a strong emphasis on streamflow analysis and forecasting, while ignoring other hydrological processes. Typical examples are the so-called distributed model inter-comparison projects (DMIP) which have been undertaken over the last decade (Smith et al., 2004, 2012). DMIP, and similar initiatives (Moreda et al., 2006; Khakbaz et al., 2012), have analysed the capacity of models to reproduce observed streamflow. It is however clear that the need of decision makers and water managers goes far beyond streamflow only. The notion that not only water in streams is relevant, but a better understanding of the full hydrological cycle is required, has led to the popular division of "blue" and "green" water (Falkenmark and Rockström, 2010). Moreover, there is a clear need that not only rainfall–runoff processes are relevant, but an integrated approach encompassing processes as glacier and snowmelt, evapotranspiration, reservoirs, changes in landcover and landuse should be better integrated in our models (Bell et al., 2014; Liu et al., 2008). Finally, the linkage with satellite remote sensing data has been shown to be very relevant to increase accuracy and usefulness of hydrological models, especially in data scarce areas (Droogers and Kite, 2002; Ines et al., 2006; Kite and Droogers, 2000; Wanders et al., 2014).

Based on the discussions above, there is a clear need for a hydrological model that combines the strengths of existing modelling approaches such that: (i) most relevant hydrological processes are integrated, (ii) setup is modular in order to switch on/off irrelevant processes and thus decreases model run-time, (iii) can relatively easily be adjusted and applied, (iv) can easily be linked to remotely sensed data, and (v) can be applied for operational as well as strategic decision support.

Over the last couple of years we have developed the Spatial Processes in Hydrology (SPHY) model and improved its usefulness by applying the model in various research projects. The objective of this publication is therefore to introduce and present the SPHY model, its development background, and demonstrate some typical applications.

Back | Close

Full Screen / Esc

Printer-friendly Version

Interactive Discussion

The model executable and source code are in the public domain (open access) and can be obtained from our website free of charge (www.sphy.nl).

2 Model overview

2.1 Introduction

The SPHY model has been developed by combining the best components of existing and well tested simulation models: HydroS (Droogers and Immerzeel, 2010), SWAT (Neitsch et al., 2009), PCR-GLOBWB (Sperna Weiland et al., 2012), SWAP (van Dam et al., 1997) and HimSim (Immerzeel et al., 2011). SPHY was developed with the explicit aim to simulate terrestrial hydrology at flexible scales, under various land use and climate conditions. SPHY is a spatially distributed leaky bucket type of model, and is applied on a cell-by-cell basis. The main terrestrial hydrological processes are described in a physically consistent way so that changes in storages and fluxes can be assessed adequately over time and space. SPHY is written in the Python programming language using the PCRaster (Karssenberg et al., 2001; Karssenberg, 2002; Karssenberg et al., 2010; Schmitz et al., 2009, 2013) dynamic modelling framework.

SPHY is grid-based and cell values represent averages over a cell (Fig. 1). For glaciers, sub-grid variability is taken into account: a cell can be glacier-free, partially glacierized, or completely covered by glaciers. The cell fraction not covered by glaciers consists of either land covered with snow or land that is free of snow. Land that is free of snow can consist of vegetation, bare soil, or open water. The dynamic vegetation module accounts for a time-varying fractional vegetation coverage, which affects processes such as interception, effective precipitation, and potential evapotranspiration. Figure 2 provides a schematic overview of the SPHY model concepts.

The land compartment is divided in two upper soil stores and a third groundwater store, with their corresponding drainage components: surface runoff, lateral flow and base flow. SPHY simulates for each cell precipitation in the form of rain or snow,

depending on the temperature. Any precipitation that falls on land surface can be intercepted by vegetation and in part or in whole be evaporated. The snow storage is updated with snow accumulation and/or snow melt. A part of the liquid precipitation is transformed in surface runoff, whereas the remainder infiltrates into the soil. The re-
5   sulting soil moisture is subject to evapotranspiration, depending on the soil properties and fractional vegetation cover, while the remainder contributes to river discharge by means of lateral flow from the first soil layer, and baseflow from the groundwater layer.

Melting of glacier ice contributes to the river discharge by means of a slow and fast component, being (i) percolation to the groundwater layer that eventually becomes
10   baseflow, and (ii) direct runoff. The cell-specific runoff, which becomes available for routing, is the sum of surface runoff, lateral flow, baseflow, snow melt and glacier melt.

If no lakes are present, then the user can choose for a simple flow accumulation routing scheme: for each cell the accumulated amount of water that flows out of the cell into its neighboring downstream cell is calculated. This accumulated amount is
15   the amount of water in the cell itself plus the amount of water in upstream cells of the cell. For each cell, the following procedure is performed: using the local drain direction network the catchment of a cell is determined which is made up the cell itself and all cells that drain to the cell. If lakes are present, then the fractional accumulation flux routing scheme is used: depending on the actual lake storage, a fraction of that storage
20   becomes available for routing and is extracted from the lake, while the remaining part becomes the updated actual lake storage. The flux available for routing is routed in the same way as in the simple flow accumulation routing scheme.

As input SPHY requires data on state variables as well as dynamic variables. For the state variables the most relevant are: Digital Elevation Model (DEM), land use type,
25   glacier cover, lakes/reservoirs and soil characteristics. The main dynamic variables are climate data such as precipitation, temperature, and reference evapotranspiration. Since SPHY is grid-based, optimal use of remote sensing data and global data sources can be made. For example, the Normalized Difference Vegetation Index (NDVI) (Tucker, 1979; Carlson and Ripley, 1997; Myneni and Williams, 1994) can be used to determine

the Leaf Area Index (LAI) in order to estimate the growth-stage of land cover. For setting-up the model, data on streamflows are not necessary. However, to undertake a proper calibration and validation procedure flow data are required. The model could also be calibrated using actual evapotranspiration, soil moisture contents, and/or snow coverage.

The SPHY model provides a wealth of output data that can be selected based on the preference of the user. Spatial output can be presented as maps of all the hydrological processes. Maps that can be displayed as output include actual evapotranspiration, runoff generation (separated by its components), and groundwater recharge. These maps can be generated on daily base, but most users prefer to get those at monthly or annual aggregated time periods. Time-series can be generated for each location in the study area. Time-series often used are stream flow under current and future conditions, actual evapotranspiration and recharge to the groundwater.

2.2 Modules

SPHY enables the user to turn on/off modules that are not required. This concept is very useful if the user is studying hydrological processes in regions where not all hydrological processes are relevant. A user may for example be interested in studying irrigation water requirements in central Africa. For this region glacier and snow melting processes are less relevant, and can thus be switched off. Another user may only be interested in simulating moisture conditions in the first soil layer, allowing the possibility to switch off the routing and groundwater modules. The advantages of turning off irrelevant modules are two-fold: (i) decrease model run-time, and (ii) decrease the amount of required model input data.

Figure 3 represents an overview of the six modules available: glaciers, snow, groundwater, dynamic vegetation, simple routing, and lake/reservoir routing. All modules can run independently from each other, except for the glaciers module. If glaciers are present, then snow processes are relevant as well (Verbunt et al., 2003; Singh and Kumar, 1997), meaning that the snow module is turned on automatically if the glaciers

Printer-friendly Version

Interactive Discussion

module is turned on. Since melting glacier water percolates to the groundwater layer, the glaciers module cannot run with the groundwater module turned off. For routing two modules are available, being (i) a simple flow accumulation routing scheme, and (ii) a fractional flow accumulation routing scheme used when lakes/reservoirs are present.

5 The user has the option to turn off routing, or to choose between one of these two routing modules. All hydrological processes incorporated in the SPHY model are described in detail in the following sections.

2.3 Reference and potential evapotranspiration

Various methods exist to calculate the reference evapotranspiration (ET_r). From the

10 many existing methods, the FAO-56 application of the Penman–Monteith equation (Allen et al., 1998) has been most widely used, and can be considered as a sort of standard (Walter et al., 2001). Despite the good physical underlying theory of this method, its major drawback is its relatively high data demand. The Penman–Monteith equation requires air temperature, windspeed, relative humidity, and solar radiation data.

15 In many regions around the world (e.g. Africa), these data are not readily measured at meteorological stations, and therefore not suitable. Another well-known method to calculate the ET_r is the Hargreaves method (Hargreaves and Samani, 1985). Droogers and Allen (2002) showed that in many regions around the globe, the Hargreaves and Penman–Monteith method showed comparable results. A lack of meteorological data

20 brought (Hargreaves and Samani, 1985) to derive the modified Hargreaves equation that is only based on the average, minimum, and maximum daily air temperature. For this reason, this equation has also been implemented in the SPHY model, according to:

$$ET_r = 0.0023 \cdot 0.408 \cdot Ra(T_{avg} + 17.8) \cdot TD^{0.5} \tag{1}$$

25 with Ra [$MJ\,m^{-2}\,d^{-1}$] the extraterrestrial radiation, T_{avg} [°C] the average daily air temperature, and TD [°C] the temperature range, defined as the difference between the

daily maximum and minimum air temperature. The constant 0.408 is required to convert the radiation to mm evaporation equivalents, and Ra can be obtained from tables (Allen et al., 1998) or equations using the day of the year and the latitude of the area of interest.

According to Allen et al. (1998), the ET_r is the evapotranspiration rate from a reference surface, not short of water. The reference surface is a hypothetical grass reference crop with specific characteristics. The potential evapotranspiration ET_p has no limitations on crop growth or evapotranspiration from soil water and salinity stress, crop density, pests and diseases, weed infestation or low fertility. Allen et al. (1998) determined the ET_p by the crop coefficient approach, where the effect of various weather conditions are incorporated into ET_r, and the crop characteristics in the crop coefficient (Kc), using:

$$ET_{p,t} = ET_{r,t} \cdot Kc \tag{2}$$

with $ET_{p,t}$ [mm] the potential evapotranspiration on day t, $ET_{r,t}$ [mm] the reference evapotranspiration on day t, and Kc [–] the crop coefficient. The effect of both crop transpiration and soil evaporation are integrated into the Kc.

If the dynamic vegetation module in SPHY is not used, then the user can opt to use a single constant Kc throughout the entire simulation period or use a time-series of crop coefficients as model input. However, vegetation is generally very dynamic throughout the year, and therefore it is not very realistic to use a single constant Kc throughout the entire simulation period. It is therefore more realistic to use a time-series of crop coefficients as model input, or use the dynamic vegetation module instead. This can be adjusted according to the user's preferences.

The Kc can be estimated using remotely sensed data (Rafn et al., 2008). In the dynamic vegetation module the Kc is scaled throughout the year using the NDVI and the maximum and minimum values for Kc, which are crop specific. These values for Kc

can easily be obtained from Allen et al. (1998). Then the Kc is calculated using:

$$Kc = Kc_{min} + (Kc_{max} - Kc_{min}) \cdot \frac{(NDVI - NDVI_{min})}{(NDVI_{max} - NDVI_{min})} \qquad (3)$$

with $NDVI_{max}$ [–] and $NDVI_{min}$ [–] the maximum and minimum values for the NDVI (vegetation type dependent). Using this approach in SPHY to calculate the Kc dynamically, using the NDVI as input, shows the strong linkage with the use of remote sensing data as input to improve model accuracy.

2.4 Dynamic vegetation processes

2.4.1 Canopy storage

SPHY allows the user to use the dynamic vegetation module in order to incorporate a time-variable vegetation cover and corresponding rainfall interception. In order to calculate the rainfall interception, the canopy storage needs to be calculated, using a time-series of the Normalized Difference Vegetation Index (NDVI) (Carlson and Ripley, 1997). The first step involves the calculation of the fraction photosynthetically active radiation (FPAR). The FPAR can be calculated using a relation between the NDVI and the FPAR, which was found by Peng et al. (2012) and described by Sellers et al. (1996), according to:

$$FPAR = min\left(\frac{(SR - SR_{min})(FPAR_{max} - FPAR_{min})}{(SR_{max} - SR_{min})} + FPAR_{min}, 0.95\right) \qquad (4)$$

with:

$$SR = \frac{1 + NDVI}{1 - NDVI} \qquad (5)$$

and $FPAR_{max}$ [–] and $FPAR_{min}$ [–] having values of 0.95 and 0.001, respectively. An FPAR of 0.95 is equivalent to the maximum LAI for a particular class, and an FPAR of

0.001 is equivalent to a minimum LAI. In order to calculate the FPAR, an NDVI time-series is required.

The second step is the calculation of the Leaf-Area-Index (LAI), which is eventually required to calculate the maximum canopy storage ($Scan_{max}$). According to Monteith (1973), the LAI for vegetation that is evenly distributed over a surface can be calculated using a logarithmic relation between the LAI and FPAR, according to:

$$LAI = LAI_{max} \cdot \frac{\log(1 - FPAR)}{\log(1 - FPAR_{max})} \tag{6}$$

with LAI [–] the Leaf-Area-Index, and LAI_{max} [–] the maximum Leaf-Area-Index (vegetation type dependent). This means that the maximum and minimum LAI values are related to the maximum and minimum of FPAR. Table 1 shows the LAI_{max} values for a certain number of vegetation types.

For vegetation that is concentrated in clusters the linear relation from Goward and Huemmrich (1992) is often used. However, since SPHY is generally applied using grid cell resolutions between 250 m and 1 km, we can assume that the effect of having vegetation concentrated in clusters is neglectable. Therefore, the calculation of the LAI in SPHY is done using the logarithmic relation of Monteith (1973) (Eq. 6).

The next step involves the calculation of the maximum canopy storage ($Scan_{max}$ [mm]). Many different relations between $Scan_{max}$ and the LAI can be found in literature depending on the vegetation type (de Jong and Jetten, 2010). The best results for crop canopies are shown by Kozak et al. (2007) and are archived by Von Hoyningen-Huene (1981) who derived the following relation between $Scan_{max}$ and the LAI:

$$Scan_{max} = 0.935 + 0.498LAI - 0.00575LAI^2 \tag{7}$$

Note that even with an LAI of zero, $Scan_{max}$ is still close to 1 mm.

2.4.2 Interception

Interception is calculated on a daily basis if the dynamic vegetation module is used, and consists of the daily precipitation plus the intercepted water remaining in the canopy storage from the previous day. First of all the canopy storage is updated with the amount of precipitation of the current day:

$$\text{Scan}_t = \text{Scan}_{t-1} + P_t \tag{8}$$

with Scan_t [mm] the canopy storage on day t, Scan_{t-1} [mm] the canopy storage on day $t-1$, and P_t [mm] the amount of precipitation on day t. The portion of precipitation that cannot be stored in the canopy storage is known as precipitation throughfall, or effective precipitation, according to:

$$\text{Pe}_t = \max(0, \text{Scan}_t - \text{Scan}_{\max,t}) \tag{9}$$

with Pe_t [mm] the effective precipitation on day t, and Scan_t [mm] the canopy storage on day t. This equation shows that precipitation throughfall only occurs if the water stored in the canopy exceeds the maximum canopy storage. After the effective precipitation has been calculated, the canopy storage is updated as:

$$\text{Scan}_t = \text{Scan}_t - \text{Pe}_t \tag{10}$$

The remaining amount of water stored in the canopy is available for interception, and the amount of water that will be intercepted depends on the atmospheric demand for open water evaporation. A commonly used value for the atmospheric demand for open water evaporation is 1.5 (Allen et al., 1998), which is derived from the ratio between one and the mean pan evaporation coefficient Kp (~ 0.65). If desired this value can easily be altered in the model code. The interception can now be calculated using:

$$\text{Int}_t = \min(1.5\text{ET}_{r,t}, \text{Scan}_t) \tag{11}$$

with Int_t [mm] the intercepted water on day t, and $\text{ET}_{r,t}$ [mm] the reference evapotranspiration on day t. Finally, the canopy storage is updated by subtracting the interception:

$$\text{Scan}_t = \text{Scan}_t - \text{Int}_t \tag{12}$$

2.5 Snow processes

For each cell a dynamic snow storage is simulated at a daily time step, adopted from on the model presented by Kokkonen et al. (2006). The model keeps track of a snow storage, which is fed by precipitation and generates runoff from snow melt. Refreezing of snow melt and rainfall within the snowpack are simulated as well.

2.5.1 Snow and rainfall

Depending on a temperature threshold, precipitation is defined to fall in either solid or liquid state. Daily snow accumulation, which is defined as solid precipitation, is calculated as:

$$P_{s,t} = \begin{cases} \text{Pe}_t & \text{if } T_{\text{avg},t} \leq T_{\text{crit}} \\ 0 & \text{if } T_{\text{avg},t} > T_{\text{crit}} \end{cases} \tag{13}$$

with $P_{s,t}$ [mm] the snowfall on day t, Pe_t [mm] the effective precipitation on day t, $T_{\text{avg},t}$ [°C] the mean air temperature on day t, and T_{crit} [°C] a calibrated temperature threshold for precipitation to fall as snow. The precipitation that falls as rain is defined as liquid precipitation, and is calculated as:

$$P_{l,t} = \begin{cases} \text{Pe}_t & \text{if } T_{\text{avg},t} > T_{\text{crit}} \\ 0 & \text{if } T_{\text{avg},t} \leq T_{\text{crit}} \end{cases} \tag{14}$$

with $P_{l,t}$ [mm] being the amount of rainfall on day t.

2.5.2 Snow melt, refreezing, and storage

To simulate snow melt, the well-established and widely used degree day melt modeling approach is used (Hock, 2003). The application of degree-day models is widespread in cryospheric models and is based on an empirical relationship between melt and air temperature. Degree-day models are easier to set up compared to energy-balance models, and only require air temperature, which is mostly available and relatively easy to interpolate (Hock, 2005). Using a degree-day modeling approach, the daily potential snow melt is calculated as follows:

$$
A_{\text{pot},t} = \begin{cases} T_{\text{avg},t} \cdot \text{DDF}_\text{s} & \text{if } T_{\text{avg},t} > 0 \\ 0 & \text{if } T_{\text{avg},t} \leq 0 \end{cases} \tag{15}
$$

with $A_{\text{pot},t}$ [mm] the potential snow melt on day t, and DDF_s [mm $^\circ$C^{-1} d^{-1}] a calibrated degree day factor for snow. The actual snow melt is limited by the snow store at the end of the previous day, and is calculated as:

$$
A_{\text{act},t} = \min(A_{\text{pot},t}, \text{SS}_{t-1}) \tag{16}
$$

with $A_{\text{act},t}$ [mm] the actual snow melt on day t, and SS_{t-1} [mm] the snow store on day $[t-1]$. The snow store from day $[t-1]$ is then updated to the current day t, using the actual snow melt ($A_{\text{act},t}$) and the solid precipitation ($P_{\text{s},t}$). Part of the actual snow melt refreezes within the snow pack and thus does not runoff immediately. When temperature is below the melting point, melt water that has refrozen in the snow pack during $[t-1]$ is added to the snow store as:

$$
\text{SS}_t = \begin{cases} \text{SS}_{t-1} + P_{\text{s},t} + \text{SSW}_{t-1} & \text{if } T_{\text{avg},t} < 0 \\ \text{SS}_{t-1} + P_{\text{s},t} - A_{\text{act},t} & \text{if } T_{\text{avg},t} \geq 0 \end{cases} \tag{17}
$$

with SS_t the snow store on day t, SS_{t-1} the snow store on day $[t-1]$, $P_{\text{s},t}$ the solid precipitation on day t, $A_{\text{act},t}$ the actual snow melt on day t, SSW_{t-1} the amount of refrozen melt water on day $[t-1]$. The units for all terms are mm.

The capacity of the snow pack to refreeze snow melt is characterized by introducing a calibrated water storage capacity (SSC [mm mm^{-1}]), which is the total mm water equivalent of snow melt that can refreeze per mm water equivalent of snow in the snow store. The maximum of melt water that can refreeze (SSW$_{max}$ [mm]) is thus limited by the thickness of the snow store:

$$SSW_{max,t} = SSC \cdot SS_t \qquad (18)$$

Then the amount of melt water stored in the snowpack, and that can refreeze in the next time-step, is calculated as:

$$SSW_t = \begin{cases} 0 & \text{if } T_{avg,t} < 0 \\ \min(SSW_{max,t},\ SSW_{t-1} + P_{l,t} + A_{act,t}) & \text{if } T_{avg,t} \geq 0 \end{cases} \qquad (19)$$

with SSW$_t$ the amount of melt water in the snow pack on day t, SSW$_{max,t}$ the maximum of melt water that can refreeze on day t, SSW$_{t-1}$ the amount of refrozen melt water on day [$t - 1$], $P_{l,t}$ the amount of rainfall on day t, and $A_{act,t}$ the actual snow melt on day t. The units of all terms are in mm.

The total snow storage (SST [mm]) consists of the snow store and the melt water that has refrozen within it, according to:

$$SST_t = (SS_t + SSW_t) \cdot (1 - GlacF) \qquad (20)$$

with $(1 - GlacF)$ [–] the gridcell fraction not covered with glaciers. In SPHY it is therefore assumed that snow accumulation and melt can only occur on the gridcell fraction determined as land surface. Snow falling on glaciers is incorporated in the glacier module.

2.5.3 Snow runoff

Runoff from snow (SRo [mm]) is generated when the air temperature is above melting point and no more melt water can be refrozen within the snow pack, according to:

$$
\text{SRo}_t = \begin{cases} A_{\text{act},t} + P_{\text{l},t} - \Delta\text{SSW} & \text{if } T_{\text{avg},t} > 0 \\ 0 & \text{if } T_{\text{avg},t} \leq 0 \end{cases} \tag{21}
$$

with ΔSSW [mm] the change in melt water stored in the snowpack according to:

$$
\Delta\text{SSW} = \text{SSW}_t - \text{SSW}_{t-1} \tag{22}
$$

2.6 Glacier processes

Since the SPHY model usually operates at a spatial resolution between 250 m and 1 km, the dynamics of glaciers such as ice flow cannot be resolved explicitly. Therefore, glaciers in SPHY are considered as melting surfaces which can completely or partly cover a grid cell.

2.6.1 Glacier melt

Glacier melt is calculated with a degree day modeling approach as well (Hock, 2005). Because glaciers covered with debris melt at different rates than debris-free glaciers (Reid et al., 2012), a distinction can be made between different degree day factors for both types. The daily melt from debris free glaciers (A_{CI} [mm]) is calculated as:

$$
A_{\text{CI},t} = \begin{cases} T_{\text{avg},t} \cdot \text{DDF}_{\text{CI}} \cdot F_{\text{CI}} & \text{if } T_{\text{avg},t} > 0 \\ 0 & \text{if } T_{\text{avg},t} \leq 0 \end{cases} \tag{23}
$$

with DDF_{CI} [mm °C^{-1} d^{-1}] a calibrated degree day factor for debris free glaciers and F_{CI} [–] is the fraction of debris free glaciers within the fractional glacier cover (GlacF)

of a grid cell. The daily melt from debris covered glaciers (A_{DC} [mm]) is calculated in a similar way, but with a different degree day factor:

$$A_{DC,t} = \begin{cases} T_{avg,t} \cdot DDF_{DC} \cdot F_{DC} & \text{if } T_{avg,t} > 0 \\ 0 & \text{if } T_{avg,t} \leq 0 \end{cases} \tag{24}$$

where DDF_{DC} [mm $°C^{-1}$ d^{-1}] is a degree day factor for debris covered glaciers and F_{DC} [–] is the fraction of debris covered glaciers within the fractional glacier cover of a grid cell. The total glacier melt per grid cell (A_{GLAC} [mm]) is then calculated by summing the melt from the debris-covered and debris-free glacier types and multiplying by the fractional glacier cover, according to:

$$A_{GLAC,t} = (A_{CI,t} + A_{DC,t}) \cdot GlacF \tag{25}$$

2.6.2 Glacier runoff

In SPHY a fraction of the glacier melt percolates to the ground water while the remaining fraction runs off. The distribution of both is defined by a calibrated glacier melt runoff factor (GlacROF [–]) which can have any value ranging from 0 to 1. Thus the generated runoff GRo [mm] from glacier melt is defined as:

$$GRo_t = A_{GLAC,t} \cdot GlacROF \tag{26}$$

2.6.3 Glacier percolation

The percolation from glacier melt to the groundwater (G_{perc} [mm]) is defined as:

$$G_{perc,t} = A_{GLAC,t} \cdot (1 - GlacROF) \tag{27}$$

The glacier water that percolates to the groundwater is added to the water percolating from the soil layers of the non-glacierized part of the grid cell (Sects. 2.7.1 and 2.7.6) which will then recharge the groundwater.

2.7 Soil water processes

2.7.1 Soil water balances

The soil water processes in SPHY are modelled for three soil layers (Fig. 2), being (i) the first soil layer (rootzone), (ii) second soil layer (subzone), and (iii) third soil layer (groundwater layer). The water balance of the first soil layer is:

$$SW_{1,t} = SW_{1,t-1} + Pe_t - Ea_t - RO_t - LF_{1,t} - Perc_{1,t} + Cap_t \tag{28}$$

with $SW_{1,t}$ and $SW_{1,t-1}$ the water content in the first soil layer on day t and $[t-1]$, respectively, Pe_t the effective precipitation on day t, Ea_t the actual evapotranspiration on day t, RO_t the surface runoff on day t, $LF_{1,t}$ the lateral flow from the first soil layer on day t, $Perc_{1,t}$ percolation from the first to the second soil layer on day t, Cap_t capillary rise from the second to the first soil layer on day t. The second soil layer water balance is:

$$SW_{2,t} = SW_{2,t-1} + Perc_{1,t} - Perc_{2,t} - Cap_t \tag{29}$$

with $SW_{2,t}$ and $SW_{2,t-1}$ the water content in the second soil layer on day t and $[t-1]$, respectively, and $Perc_{2,t}$ percolation from the second to the third soil layer on day t. The third soil layer water balance is given as:

$$SW_{3,t} = SW_{3,t-1} + Gchrg_t - BF_t \tag{30}$$

with $SW_{3,t}$ and $SW_{3,t-1}$ the water content in the third soil layer on day t and $[t-1]$, respectively, $Gchrg_t$ groundwater recharge from the second to the third soil layer on day t, and BF_t baseflow on day t. If the glacier module is used, then groundwater recharge consists of percolation from the second soil layer and percolated glacier melt, otherwise only percolation from the second soil layer is taken into account.

The user can opt to run SPHY without the third soil layer (groundwater). This may be desirable if the user for example is mainly interested in simulating soil moisture

conditions in the rootzone, instead of evaluating e.g. the contribution of baseflow to the total routed river flow. In that case only the two upper soil layers are used where the bottom boundary of soil layer two is controlled by a seepage flux (pos. outward), and instead of baseflow from the third soil layer, water leaves the second soil layer through lateral flow. With the groundwater module turned off, the water balance for the second soil layer is:

$$SW_{2,t} = SW_{2,t-1} + Perc_{1,t} - LF_{2,t} - Cap_t - Seep \tag{31}$$

with $LF_{2,t}$ lateral flow from the second soil layer, and Seep seepage in or out of the second soil layer (pos. is outgoing). The units for all water balance terms are mm.

2.7.2 Actual evapotranspiration

Evapotranspiration refers to both the transpiration from vegetation and the evaporation from soil or open water. As was mentiond in Sect. 2.3, the Kc accounts for both the crop transpiration and soil evaporation. The additional use of the dynamic vegetation module accounts for a time-variable vegetation cover, meaning that the role of evaporation becomes more dominant as soons as vegetation cover decreases.

Many limiting factors (e.g. salinity stress, water shortage, water excess, diseases) can cause a reduction in potential evpotranspiration (ET_p), resulting in the actual evapotranspiration rate (ET_a). Since SPHY is a water-balance model, SPHY only accounts for stresses related to water shortage or water excess. If there is too much water in the soil profile, then the plant is unable to extract water because of oxygen stress (Bartholomeus et al., 2008). The calculation of evapotranspiration reduction due to water excess (oxygen stress) is quite complex and requires a vast amount of parameters that is generally not available for the spatial scale that SPHY is applied on. Therefore, SPHY uses a evapotranspiration reduction parameter ($ETred_{wet}$) that has a value of 0 if the soil is saturated, and otherwise it will have a value of 1. This parameter is used in the following equation to calculate the actual evapotranspiration:

$$ET_{a,t} = ET_{p,t} \cdot ETred_{wet} \cdot ETred_{dry} \tag{32}$$

with $ET_{a,t}$ [mm] the actual evapotranspiration on day t, $ET_{p,t}$ [mm] the potential evapotranspiration on day t, and $ETred_{wet}$ and $ETred_{dry}$ being the reduction parameters for water excess and water shortage conditions, respectively. The $ETred_{dry}$ is calculated using the Feddes equation (Feddes et al., 1978), which assumes a linear decline in rootwater uptake if the water pressure head drops below a critical value. This critical value can be determined using the soil water retention curve (pF-curve), which relates the soil type to its water binding capacity. This binding capacity is a suction force, and is often expressed in cm negative water column. The pF is simply calculated as:

$$pF = \log_{10}(-H) \tag{33}$$

with H [cm] the soil water pressure. Soils that are at field capacity generally have a pF of 2, meaning -100 cm of water column, and soils that are at permanent wilting point have a pF of 4.2, or $-16\,000$ cm of water column. The permanent wilting point is often referred to as the point where the crop dies. In SPHY it is assumed that the linear decline in rootwater uptake starts at a pF of 3 (-1000 cm water column). Therefore, the $ETred_{dry}$ [–] is calculated as:

$$ETred_{dry,t} = \frac{SW_{1,t} - SW_{1,pF4.2}}{SW_{1,pF3} - SW_{1,pF4.2}} \tag{34}$$

with $ETred_{dry,t}$ [–] the reduction in rootwater uptake due to water shortage on day t, $SW_{1,t}$ [mm] the actual soil water content in the first soil layer on day t, and $SW_{1,pF3}$ [mm] and $SW_{1,pF4}$ [mm] the soil water content in the first soil layer at pF3 and pF4, respectively. $ETred_{dry}$ can therefore have values ranging between zero and one, where a value of one represents optimal plant growing conditions, and zero means no rootwater uptake at all. Using $ETred_{dry}$ in Eq. (32) to calculate ET_a

2.7.3 Surface runoff

Within the field of hydrology two types of surface runoff can be distinguished: Hewlettian (Hewlett, 1961) and Hortonian (Beven, 2004; Corradini et al., 1998) runoff. Hewlettian

Title Page

Abstract | Introduction

Conclusions | References

Tables | Figures

|◀ | ▶|

◀ | ▶

Back | Close

Full Screen / Esc

Printer-friendly Version

Interactive Discussion

runoff is often referred to as saturation excess overland flow, while Hortonian runoff is also known as infiltration excess overland flow. Hewlettian runoff occurs when the soil is saturated, and more rainfall is added, resulting in direct surface runoff. Hortonian runoff occurs when the rainfall intensity exceeds the infiltration capacity of the soil: during wetting of the soil, the soil infiltration capacity decreases over time, and if at a certain moment the rainfall intensity exceeds the soil infiltration capacity, surface runoff occurs.

Since the SPHY model runs on a daily time-step, the model does not account for sub-daily variability in rainfall intensities, meaning that Hortonian runoff processes can be considered as less important. For this reason SPHY uses the Hewlettian runoff concept to calculate surface runoff. Surface runoff is calculated from the first soil layer:

$$RO = \begin{cases} SW_1 - SW_{1,sat} & \text{if } SW_1 > SW_{1,sat} \\ 0 & \text{if } SW_1 \leq SW_{1,sat} \end{cases} \tag{35}$$

with RO [mm] surface runoff, SW_1 [mm] the water content in the first soil layer, and $SW_{1,sat}$ [mm] the saturated water content of the first soil layer.

2.7.4 Lateral flow

Lateral flow is substantial in catchments with steep gradients and soils with high hydraulic conductivities (Beven, 1981; Beven and Germann, 1982; Sloan and Moore, 1984). In SPHY it is assumed that only the amount of water exceeding field capacity can be used for lateral flow. Therefore, first the drainable volume of water (excess water) needs to be calculated:

$$W_{l,exc} = \begin{cases} SW_l - SW_{l,fc} & \text{if } SW_l > SW_{l,fc} \\ 0 & \text{if } SW_l \leq SW_{l,fc} \end{cases} \tag{36}$$

with $W_{l,exc}$ [mm] the drainable volume of water from soil layer l, SW_l [mm] the water content in soil layer l, and $SW_{l,fc}$ [mm] the field capacity of soil layer l. According to

Sloan and Moore (1984), the lateral flow at the hillslope outlet can be calculated as:

$$LF_l^* = W_{l,\text{excfrac}} \cdot v_{\text{lat},l} \tag{37}$$

with LF_l^* [mm] lateral flow from soil layer l, $W_{l,\text{excfrac}}$ [–] the drainable volume of water as fraction of the saturated volume, and $v_{\text{lat},l}$ [mm d^{-1}] the flow velocity at the outlet. In SPHY, the drainable volume as fraction of the saturated volume is calculated as:

$$W_{l,\text{excfrac}} = \frac{W_{l,\text{exc}}}{SW_{l,\text{sat}} - SW_{l,\text{fc}}} \tag{38}$$

The velocity of flow at the outlet, $v_{\text{lat},l}$ [mm d^{-1}], depends on both the saturated hydraulic conductivity $K_{\text{sat},l}$ [mm d^{-1}] and the slope of the hill slp [–], and is defined as:

$$v_{\text{lat},l} = K_{\text{sat},l} \cdot \text{slp} \tag{39}$$

The slope (slp) in SPHY is calculated for each gridcell as the increase in elevation per unit distance.

According to Neitsch et al. (2009), only a fraction of lateral flow will reach the main channel on the day it is generated if the catchment of interest is large with a time of concentration is greater than 1 day. This concept is also implemented in the SPHY model, and uses a lateral flow travel time $TT_{\text{lag},l}$ [d] to lag a portion of lateral flow release to the channel:

$$LF_l = \left(LF_l^* + LF_{l,t-1}^* \right) \cdot \left(1 - \exp\left[\frac{-1}{TT_{\text{lag},l}} \right] \right) \tag{40}$$

with LF_l [mm] the amount of lateral flow entering the channel on a given day, LF_l^* [mm] the lateral flow (Eq. 37) generated within the cell on a given day, $LF_{l,t-1}^*$ [mm] the lateral flow lagged from the previous day. SPHY assumes the lateral flow travel time to

be dependent on the field capacity $SW_{l,fc}$ [mm], saturated content $SW_{l,sat}$ [mm], and the saturated conductivity $K_{sat,l}$ [mm d^{-1}], according to:

$$TT_{lag,l} = \frac{SW_{l,sat} - SW_{l,fc}}{K_{sat,l}} \tag{41}$$

A larger lateral flow travel time will result in a smoother streamflow hydrograph.

2.7.5 Percolation

If the groundwater module is used, then water can percolate from the first to the second soil layer, and from the second to the third soil layer. If the user decides to run SPHY without the groundwater module, percolation only occurs from the first to the second soil layer. In SPHY water can only percolate if the water content exceeds the field capacity of that layer, and the water content of the underlying layer is not saturated. A similar approach has been used in the SWAT model (Neitsch et al., 2009). The water volume available for percolation to the underlying layer is calculated as:

$$W_{l,exc} = \begin{cases} 0 & \text{if } SW_l \leq SW_{l,fc} \text{ or } SW_{l+1} \geq SW_{l+1,sat} \\ SW_{l+1,sat} - SW_{l+1} & \text{if } SW_l - SW_{l,fc} > SW_{l+1,sat} - SW_{l+1} \\ SW_l - SW_{l,fc} & \text{else} \end{cases} \tag{42}$$

with $W_{l,exc}$ [mm] the drainable volume of water from layer l, SW_l [mm] the water content in layer l, $SW_{l,fc}$ [mm] field capacity of layer l, SW_{l+1} [mm] the water content in layer $[l + 1]$, and $SW_{l+1,sat}$ [mm] the saturated water content of layer $[l + 1]$. Only a certain amount of $W_{l,exc}$ will percolate to the underlying soil layer, depending on the percolation travel time $TT_{perc,l}$ [d]. This approach follows the storage routing methodology, which is also implemented in the SWAT model (Neitsch et al., 2009):

$$w_{l,perc} = W_{l,exc} \cdot \left(1 - \exp\left[\frac{-1}{TT_{perc,l}} \right] \right) \tag{43}$$

with $w_{l,\text{perc}}$ [mm] the amount of water percolating to the underlying soil layer. The travel time for percolation is calculated in the same way as the travel time for lateral flow (Eq. 41).

2.7.6 Groundwater recharge

Water that percolates from the second to the third soil layer will eventually reach the shallow aquifer. This process is referred to as groundwater recharge hereafter. If the glacier module is used as well, then also glacier melt that percolates contributes to the groundwater recharge. Groundwater recharge often does not occur instantaneous, but with a time lag that depends on the depth of the groundwater table and soil characteristics. SPHY uses the same exponential decay weighting function as proposed by Venetis (1969) and used by Sangrey et al. (1984) in a precipitation groundwater response model. This approach has also been adopted in the SWAT model (Neitsch et al., 2009), using:

$$\text{Gchrg}_t = \left(1 - \exp^{\frac{-1}{\delta_{\text{gw}}}}\right) \cdot w_{2,\text{perc}} + \exp^{\frac{-1}{\delta_{\text{gw}}}} \cdot \text{Gchrg}_{t-1} \tag{44}$$

with Gchrg_t [mm] and Gchrg_{t-1} [mm] the groundwater recharge on day t and $t-1$, respectively. δ_{gw} [d] is the delay time and $w_{2,\text{perc}}$ [mm] is the amount of water that percolates from the second to the third layer on day t.

2.7.7 Baseflow

After groundwater recharge has been calculated, SPHY calculates baseflow which is defined as the flow going from the shallow aquifer to the main channel. Baseflow only occurs when the amount of water stored in the third soil layer exceeds a certain threshold ($\text{BF}_{\text{thresh}}$) that can be specified by the user. Baseflow calculation in SPHY is based on the steady-state response of groundwater flow to recharge (Hooghoudt, 1940) and the water table fluctuations that are a result of the non-steady response of groundwater flow to periodic groundwater recharge (Smedema and Rycroft, 1983). The SWAT

model (Neitsch et al., 2009) assumes a linear relation between the variation in groundwater flow (baseflow) and the rate of change in water table height, according to:

$$\frac{dBF}{dt} = 10 \cdot \frac{K_{sat}}{\mu L_{gw}^2} \cdot (Gchrg - BF) = \alpha_{gw} \cdot (Gchrg - BF) \tag{45}$$

with BF [mm] the groundwater flow (baseflow) into the main channel on day t, K_{sat} [mm d^{-1}] the hydraulic conductivity of the shallow aquifer, μ [–] the specific yield of the shallow aquifer, L_{gw} [m] the distance from the subbasin divide for the groundwater system to the main channel, Gchrg [mm] the amount of groundwater (Eq. 44) recharge entering the shallow aquifer on day t, and α_{gw} [–] is the baseflow recession coefficient. Equation (45) can be integrated and rearranged to calculate baseflow, according to:

$$BF_t = \begin{cases} 0 & \text{if } SW_3 \leq BF_{thresh} \\ BF_{t-1} \cdot \exp^{-\alpha_{gw}} + Gchrg_t \cdot \left(1 - \exp^{-\alpha_{gw}}\right) & \text{if } SW_3 > BF_{thresh} \end{cases} \tag{46}$$

with BF_t [mm] the baseflow into the channel on day t, and BF_{t-1} [mm] the baseflow into the channel on day $t - 1$. Since this equation has proven its succes in the SWAT model (Neitsch et al., 2009) throughout many applications worldwide, this equation has been adopted in the SPHY model as well.

The baseflow recession coefficient (α_{gw}) is an index that relates the baseflow response to changes in groundwater recharge. Lower values for α_{gw} therefore correspond to areas that respond slowly to groundwater recharge, whereas higher values indicate areas that have a rapid response to groundwater recharge. The baseflow recession coefficient is generally used as a calibration parameter in the SPHY model, but a good first approximation of this coefficient can be calculated using the number of baseflow days (Neitsch et al., 2009):

$$\alpha_{gw} = \frac{2.3}{BFD} \tag{47}$$

with BFD [d] the number of baseflow days, which is defined as the number of days required for baseflow recession to decline.

Full Screen / Esc

Printer-friendly Version

Interactive Discussion

2.8   Streamflow routing

After calculating the different runoff components, the cell specific total runoff (QTot) is calculated by summarizing these different runoff components. Depending on the modules being switched on, the different runoff components are (i) rain runoff (RRo), (ii) snow runoff (SRo), (iii) glacier runoff (GRo), and (iv) baseflow (BF). If the groundwater module is not used, then baseflow is calculated as being the lateral flow from the second soil layer. Rainfall runoff is the sum of surface runoff (RO, Sect. 2.7.3) and lateral flow from the first soil layer (LF$_1$, Sect. 2.7.4). Then QTot is calculated according to:

$$QTot = RRo + SRo + GRo + BF \tag{48}$$

with QTot [mm] the cell specific total runoff, RRo [mm] rainfall runoff, SRo [mm] snow runoff, GRo [mm] glacier runoff, and BF [mm] being baseflow from the third soil layer or latereral flow from the second soil layer. In order to obtain river discharge, QTot needs to be routed through a flow direction network. SPHY allows the user to opt between the use of a simple routing scheme (Sect. 2.8.1), or a more complex routing scheme (Sect. 2.8.2) that involves the calculation of lake outflow through $Q(h)$ relations. Both methods require a flow direction network map, which can be obtained by delineating a river network using PCRaster or GIS software in combination with a Digital Elevation Model (DEM).

2.8.1   Routing

In hydrology streamflow routing is referred to as being the transport of water through an open channel network. Since open-channel flow is unsteady, streamflow routing often involves the solving of complex partial differential equations. The St. Venant equations (Brutsaert, 1971; Morris and Woolhiser, 1980) are often used for this, but these have high data requirements related to the river geometry and morphology, which is unavailable for the spatial scale SPHY is generally applied on. Additionally, solving these

equations require the use of very small time steps, which result in large model calculation times. Other models, such as e.g. SWAT (Neitsch et al., 2009), use the Manning equation (Manning, 1989) to define the rate and velocity of river flow in combination with the variable storage (Williams, 1975) or Muskingum (Gill, 1978) routing methods

5 to obtain river streamflow. But also the Manning equation requires river bed dimensions, which are generally unknown on the spatial scale that SPHY generally is applied on.

Therefore, SPHY calculates for each cell the accumulated amount of water that flows out of the cell into its neighbouring downstream cell. This can easily be obtained by us-

10 ing the accuflux PCRaster builtin function. If only the accuflux function would be used, then it is assumed that all the specific runoff generated within the catchment on one day will end up at the most downstream location within one day, which is not plausible. Therefore, SPHY implements a flow recession coefficient (kx [–]) that accounts for flow delay, which can be a result of channel friction. Using this coefficient, river flow in SPHY

15 is calculated using the three equations shown below:

$$QTot_t^* = \frac{QTot_t \cdot 0.001 \cdot A}{24 \cdot 3600} \tag{49}$$

$$Q_{accu,t} = accuflux\left(F_{dir}, QTot_t^*\right) \tag{50}$$

$$Q_{rout,t} = (1 - kx) \cdot Q_{accu,t} + kx \cdot Q_{rout,t-1} \tag{51}$$

with $QTot_t^*$ [m^3 s^{-1}] the specific runoff on day t, $QTot_t$ the specific runoff in mm on day t,

20 A [m^2] the grid cell area, $Q_{accu,t}$ [m^3 s^{-1}] the accumulated streamflow on day t without flow delay taken into account, $Q_{rout,t}$ [m^3 s^{-1}] the routed streamflow on day t, $Q_{rout,t-1}$ [m^3 s^{-1}] the routed streamflow on day $t-1$, F_{dir} the flow direction network, and kx [–] the flow recession coefficient. kx has values ranging between zero and one, where values close to zero correspond to a fast responding catchment, and values approacing one

25 correspond to a slow responding catchment.

The user can opt to rout each of the four streamflow contributors separately, which may be useful if one wants to evaluate for example the contribution of glacier melt or

snow melt to the total routed runoff. However, this increases model run-time substantially, because the accuflux function, which is a time consuming function, needs to be called multiple times depending on the number of flow contributors to be routed.

2.8.2 Lake/reservoir routing

Lakes or reservoirs act as a natural buffer, resulting in a delayed release of water from these water bodies. SPHY allows the user to choose a more complex routing scheme if lakes/reservoirs are located in their basin of interest. The use of this more advanced routing scheme requires a known relation between lake outflow and lake level height ($Q(h)$ relation) or lake storage.

To use this routing scheme, SPHY requires a nominal map with cells identified as lakes each have a unique ID, while the non-lake cells have a value of zero. The user can supply a boolean map with True for cells that have measured lake levels, and False for lake cells that do not have measured lake levels. This specific application of SPHY is discussed in detail in Sect. 3.3.

Four different relations can be chosen to calculate the lake outflow from the lake level height or lake storage, being: (i) an exponential relation, (ii) a first-order polynomial function, (iii) a second-order polynomial function, and (iv) a third-order polynomial function. The user needs to supply maps containing the coefficients used in the different functions.

The lake/reservoir routing scheme simply keeps track of the actual lake storage, meaning that an initial lake storage should be supplied. Instead of the simple accuflux function described in the previous section, the lake/reservoir routing scheme uses the PCRaster functions accufractionstate and accufractionflux. The accufractionflux calculates for each cell the amount of water that is transported out of the cell, while the accufractionstate calculates the amount of water that remains stored in the cell. For non-lake cells the fraction that is transported to the next cell is always equal to one, while the fraction that is transported out of a lake/reservoir cell depends on the actual lake storage. Each model time-step the lake storage is updated by inflow from

upstream. Using this updated storage, the lake level and corresponding lake outflow can be calculated using one of the four relations mentioned before. The lake outflow can then be calculated as a fraction (Q_{frac} [–]) of the actual lake storage. Instead of using Eq. (50), the Q_{frac} is then used in Eqs. (52) and (53) to calculate the accumulated streamflow and updated storage, respectively:

$$Q_{\text{accu},t} = \text{accufractionflux}(F_{\text{dir}}, S_{\text{act},t}, Q_{\text{frac},t}) \tag{52}$$

$$S_{\text{act},t+1} = \text{accufractionstate}(F_{\text{dir}}, S_{\text{act},t}, Q_{\text{frac},t}) \tag{53}$$

with $S_{\text{act},t}$ [m^3] and $S_{act,t+1}$ [m^3] the actual storage and updated storage to be used in the next time-step, respectively, and $Q_{\text{accu},t}$ [m^3 d^{-1}] the accumulated streamflow on day t, without flow delay taken into account. Since Q_{frac} is always equal to one for the non-lake cells, the accufractionflux function becomes equal to the accuflux function used in the previous section. This actually means that for the river network the same routing function from Sect. 2.8.1 is used, and that Eqs. (52) and (53) only apply to lake/reservoir cells.

In order to account for non-linearity and slower responding catchments, the same kx coefficient is used again. This involves applying Eq. (51) as a last step after Eq. (52) and converting the units from m^3 d^{-1} to m^3 s^{-1}. Since the accufractionflux and accufraction state functions are more complex to compute, the use of these functions increases model run-time.

3 Applications

The SPHY model has been applied and tested in various studies ranging from real-time soil moisture predictions in lowlands, to operational reservoir inflow forecasting applications in mountainous catchments, to irrigation scenarios in the Nile Basin, to detailed climate change impact studies in the snow-glacier-rain dominated Himalayan region. Some typical applications will be summarized in the following sections.

Full Screen / Esc

Printer-friendly Version

Interactive Discussion

3.1 Irrigation management in lowland areas

As SPHY produces spatial outputs for the soil moisture content in the root zone and the potential and actual evapotranspiration (ET), it is a useful tool for application in agricultural water management decision support. By facilitating easy integration of remote sensing data, crop growth stages can be spatially assessed at different moments in time. The SPHY dynamic vegetation module ensures that all relevant soil water fluxes correspond with crop development stages throughout the growing season. Spatially distributed maps of root water content and ET deficit can be produced, enabling both the identification of locations where irrigation is required and a quantitative assessment of crop water stress.

SPHY has been applied with the purpose of providing field-specific irrigation advice for a large-scale farm in western Romania, comprising 380 individual fields and approximately ten different crops. Contrary to the other case studies highlighted in this paper, a high spatial resolution is very relevant for supporting decisions on variable-rate irrigation. The model has therefore been set up using a 30 m resolution, covering the 2013 and 2014 cropping seasons on a daily time step. Optical satellite data from Landsat 8 (USGS, 2013) were used as input to the dynamic vegetation module. Soil properties were derived from the Harmonized World Soil Database (Batjes et al., 2012), which for Romania contains data from the Soil Geographical Database for Europe (Lambert et al., 2003). Using the Van Genuchten equation (Van Genuchten, 1980), soil saturated water content, field capacity, and wilting point were determined for the HWSD classes occurring at the study site. Elevation data was obtained from the EU-DEM dataset (EEA, 2014), and air temperature was measured by two on-farm weather stations.

In irrigation management applications, a model should be capable of simulating the moisture stress experienced by the crop due to insufficient soil moisture contents, which manifests itself by an evapotranspiration deficit (potential ET – actual ET > 0). Field measurements of soil moisture and/or actual ET are therefore desired for calibration purposes. In this case study, a capacitance soil moisture sensor was installed

on a soybean field to monitor rootzone water content shortly after 1 May 2014, which is the start of the soybean growing season. The sensor measures volumetric moisture content for every 10 cm of the soil profile up to a depth 60 cm. It is also equipped with a rain gauge measuring the sum of rainfall and applied irrigation water, which was used as an input to SPHY. Soil moisture measured over the extent covered by the crop root depth was averaged and compared to simulated values (Fig. 4).

As can be seen in Fig. 4, the temporal patterns as measured by the soil moisture sensor are well simulated by the SPHY model. Based on daily soil moisture values, a Nash–Sutcliffe (Nash and Sutcliffe, 1970) model efficiency coefficient of 0.6 was found, indicating that the quality of prediction of the uncalibrated SPHY model is "good" (Foglia et al., 2009).

The performance of the SPHY model can be improved by calibration using remotely sensed evapotranspiration (Immerzeel and Droogers, 2008), although such data is often not available on these small scales as ET is a very complex parameter to assess (Samain et al., 2012). It should also be noted that soil moisture content is typically highly variable in space; a very high correlation between point measurements and grid cell simulations of soil moisture may therefore not always be feasible (Bramer et al., 2013).

3.2 Snow and glacier-fed river basins

SPHY is being used in large Asian river basins with significant contribution of glacier- and snow melt to the total flow (Lutz et al., 2012b, a, 2014). The major goals of these applications are two-fold:

– Assess the current hydrological regimes at high-resolution; e.g. assess spatial differences in the contributions of glacier melt, snow melt and rainfall–runoff to the total flow

– Quantify the effects of climate change on the hydrological regimes in the future and how these affect the water availability

Back | Close

Full Screen / Esc

Printer-friendly Version

Interactive Discussion

Rivers originating in the high mountains of Asia are considered to be the most melt-water dependent river systems on Earth (Schaner et al., 2012). In the regions surrounding the Himalayas and the Tibetan Plateau large human populations depend on the water supplied by these rivers (Immerzeel et al., 2010). However, the dependency on melt water differs strongly between river basins as a result of differences in climate and differences in basin hypsometry (Immerzeel and Bierkens, 2012). Only by using a distributed hydrological modelling approach that includes the simulation of key hydrological and cryospheric processes, and inclusion of transient changes in climate, snow cover, glaciers and runoff, appropriate adaptation and mitigation options can be developed for this region (Sorg et al., 2012). The SPHY model is very suitable for such an approach, and has therefore been widely applied in the region.

For application in this region, SPHY was setup at a 1 km spatial resolution using a daily time-step, and forced with historical air temperature (Tavg, Tmax, Tmin) and precipitation data, obtained from global and regional datasets (e.g. APHRODITE (Yatagai et al., 2012), Princeton (Sheffield et al., 2006), TRMM (Gopalan et al., 2010)) or interpolated WMO station data from a historical reference period. For this historical reference period SPHY was calibrated and validated using observed streamflow. For the future period, SPHY was forced with downscaled climate change projections obtained from General Circulation Models (GCMs), as available through the Climate Model Intercomparison Projects (e.g. CMIP3, Meehl et al., 2007, CMIP5, Taylor et al., 2012), and which were used as basis for the Assessment Reports prepared by the Intergovernmental Panel on Climate Change (IPCC).

In Central Asia, SPHY was succesfully applied in a study (ADB, 2012; Lutz et al., 2012b, a) that focused on the impacts of climate change on water resources in the Amu Darya and Syr Darya river basins. SPHY was used to quantify the hydrological regimes in both basins, and subsequently to project the outflow from the upstream basins to the downstream areas by forcing the model with an ensemble of 5 CMIP3 GCMs. The SPHY model output fed into a water allocation model that was setup for the downstream parts of the Amu Darya and Syr Darya river basins.

In the Himalayan Climate Change Adaptation Programme (HICAP), led by the International Centre for Integrated Mountain Development (ICIMOD), SPHY has been successfully applied in the upstream basins of the Indus, Ganges, Brahmaputra, Salween and Mekong rivers (Lutz et al., 2013, 2014). In this study the hydrological regimes of these five basins have been quantified and the calibrated and validated model (Fig. 5) was forced with an ensemble of eight GCMs to create water availability scenarios until 2050. SPHY allowed the assessment of current and future contribution of glacier melt and snow melt to total flow (Fig. 6), and how total flow volumes and the intra-annual distribution of river flow will change in the future.

3.3 Flow forecasting

In harsh environments like Chile, hydropower companies have been using forecasting solutions such as statistical regressions of flow observations, or mathematical simulations with a minimum content of real-time physical information. These solutions are generally based on long historical data sets of flow observations, and do not take into account the current hydrological state of the basin and the climate for the coming weeks/months. During the INTOGENER project, the SPHY model was used to demonstrate the operational capabilities of a water flow monitoring and prediction system aimed at hydropower production and water management organizations.

The INTOGNER system uses measurements derived from both Earth Observation (EO) satellites and in-situ sensors. Data that were retrieved from EO satellites consisted of a DEM map and a map-series of snow cover. Snow cover images were retrieved on a weekly basis, using RADARSAT and MODIS (Parajka and Blöschl, 2008; Hall et al., 2002) imagery. These images were used to update the snow store (SS [mm]) in the model in order to initialize the model for the forecasting period. Discharge, precipitation and temperature data were collected using in-situ meteorological stations. In order to calculate the lake outflow accurately, the SPHY model was initialized with water level measurements retrieved from reflected Global Navigation Satellite System (GNSS) signals in Laja Lake. Static data that was used in the SPHY model consisted

of soil characteristics derived from the Harmonized World Soil Database (HWSD) (Batjes et al., 2009) and land use data obtained from the GLOBCOVER (Bontemps et al., 2011) product. The SPHY model was setup to run at a spatial resolution of 200 m.

Figure 8 shows the observed vs. simulated daily streamflow for two locations within the Laja River Basin for the historical period 2007–2008. It can be seen that model performance is quite satisfactory for both locations, with volume errors of −4 and −9.4 % for Canal Abanico (downstream of Laja Lake) and Rio Laja en Tucapel, respectively. The NS-coefficient (Nash and Sutcliffe, 1970), which is especially useful to assess the simulation of high discharge peaks, is less satisfactory for these locations. Hydropower companies, however, have more interest in expected flow volumes for the coming weeks/months than for accurate day-to-day flow simulations, and therefore the NS-coefficient is less important in this case. If the NS-coefficient is calculated for the same period on a monthly basis, then the NS-coefficients are 0.53 for Canal Abanico and 0.81 for Rio Laja en Tucapel. It is likely that SPHY model performance would even be better if a full model calibration would have been performed.

The hydropower company's main interest is the model's capacity to predict the total expected flow for the coming weeks during the melting season (October 2013 through March 2014). Figure 9 shows the bias between the total cumulative forecasted flow and observed flow for the 23 model runs that were executed during operational mode. Although there are some bias fluctuations in the Rio Laja en Tucapel model runs, it can be concluded that the bias decreases for each next model run for both locations, which is a logical result of a decreasing climate forcing uncertainty as the model progresses in time. It can be seen that the SPHY model streamflow forecasts for Canal Abanico, which is downstream of Laja Lake, are substantially better than for Rio Laja en Tucapel (most downstream location). The reason for this has not been investigated during the demonstration study, but since model performance for these two locations was satisfactory during calibration, a plausible explanation could be the larger climate forecast uncertainty in the higher altitude areas (Hijmans et al., 2005; Rollenbeck and Bendix, 2011) in the northeastern part of the basin that contributes to the streamflow of Rio

Laja en Tucapel. Additionally, only two in-situ meteorological stations were available during operational mode, whereas during calibration 20+ meteorological stations were available. Moreover, these operational meteorological stations were not installed on higher altitudes, where precipitation patterns tend to be spatially very variable (Wagner et al., 2012; Rollenbeck and Bendix, 2011).

4 Future outlook

Further development and refinement of the SPHY model are foreseen in six areas, being (i) evapotranspiration processes, (ii) depression storage, (iii) representation of lakes/reservoirs, (iv) streamflow routing, (v) cryospheric processes, and (vi) the development of a graphical user-interface.

The current version of the SPHY model calculates the reference evapotranspiration using the modified Hargreaves equation (Hargreaves and Samani, 1985), which requires three meteorological variables: the average, maximum and minimum daily air temperature. Although this method is less data demanding than the well-known Penman–Monteith (Allen et al., 1998) equation, additional methods for the calculation of the reference evapotranspiration that are even less data demanding should be explored for future versions of the SPHY model.

Besides the dynamic simulation of a time-varying fractional vegetation coverage, using NDVI time-series as input, it is currently assumed that the root depth of a growing crop is constant throughout the simulation period, and that it is equal to the depth of the first soil layer. In reality a crop is seeded, starts to develop its root system, and finally gets harvested. Although this root development process is less dynamically for forests and therefore more relevant for agricultural crops, it can be seen as an improvement to be included in the SPHY model. A similar approach as in the SWAP model (van Dam et al., 1997) could be used, where the user needs to define the root depths for each growing stage. However, it should be taken into account that the SWAP model is a field-scale model for which crop-specific root depth information is generally available,

and that SPHY is generally applied on larger spatial scales where cropping calendars, and thus corresponding root depth information is harder to obtain.

Surface runoff in SPHY occurs whenever excess rainfall results in saturation of the first soil layer. Subsequently, this excess rainfall leaves the grid-cell as surface runoff without any obstacles or friction, and enters the river system within the same day. In reality, surface runoff can be delayed because of surface friction, or stored in local depressions or man-made ponds (surface irrigation), before it is released to the river system. The concept of having a ponding layer is mainly beneficial for (i) agricultural applications where surface irrigation in combination with a ponding layer plays a major role, e.g. rice irrigation, and/or (ii) if the model is run on very high spatial resolution where the role of local depressions becomes more prominent; water can be stored for hours/days in these depressions, and water may be partly or completely evaporated before it has the chance to flow to the channels. The effect of delayed surface runoff can be related to dense vegetation or agricultural land management practices (Hunink et al., 2013; Kauffman et al., 2014), with bench terraces and contour tillage being examples of these practices. The effect of delayed or stored surface runoff is currently not implemented in the SPHY model, but should be further explored for future SPHY versions.

As was mentioned in Sect. 2.8.2, each individual lake is represented by maximum one grid-cell in SPHY. This is related to the PCRaster flow direction calculation: each cell needs to flow to a downstream cell, and the total flow in the most downstream cell should be equal to the accumulated flow of all upstream cells plus the flow generated within that cell. This means that large lakes, consisting of multiple neighboring cells, can be seen as an enormous pit in the flow direction network, meaning that streamflow routing from the upstream lake cells is interrupted at these pit cells. Since large lakes can evaporate a substantial amount of water (Gat et al., 1994), a lake-cell merging procedure should be developed for future versions of the SPHY model, that allows to automatically re-create the flow direction network based on the locations of the lake

inflow cells and outflow cell, such that all the accumulated water of the inflow cells is allocated and stored in the downstream cell, where it can continue its way downstream.

Although the currently implemented routing scheme in SPHY has proven its success during various applications (see Sects. 3.2 and 3.3), improvements in the routing scheme are foreseen for future SPHY versions. Using the current approach it is assumed that the open channel surface area equals the grid cell area. If coarse model resolutions are used, then this assumption becomes less plausible, because in reality the surface area of a river would only cover a small fraction of this grid cell area. Therefore, it would be interesting to explore using more advanced routing schemes that take into account the river's cross section dimensions and corresponding velocity flow rates. An example of a more advanced routing scheme, that takes into account the channel dimensions, and has been found to yield good results under a wide range of conditions in natural rivers (Brutsaert, 2005) is the Muskingum method (Gill, 1978). Considering the larger spatial resolutions that SPHY is generally applied for, it seems almost infeasible to determine the channel dimensions. However, some emperical relations between the bank-full dischargen and channel dimensions are available (Park, 1977), and should be explored for implementing in SPHY.

Sublimation of snow is an important component of the water balance in areas experiencing snow cover during significant time of the year (Strasser et al., 2008). Different approaches have been developed to estimate this flux in hydrological models (Bowling et al., 2004; MacDonald et al., 2009; Lenaerts et al., 2010; Groot Zwaaftink et al., 2013). Development of a parameterization of sublimation using the low data requirement of SPHY is foreseen.

In SPHY, glaciers are considered as entities generating melt using a temperature-index model. Improvements in the representation of glaciers are foreseen to make them mass-conserving, e.g. considering the precipitation falling in their accumulation areas. In the current SPHY version, all surface runoff that is generated on glacier covered areas is considered as glacier melt, and inclusion of further specification to seasonal snow melt and glacier ice melt is foreseen. Besides, the temperature-index model can

be improved by including the incoming radiation in addition to air temperature in the temperature-index model (Hock, 2003; Pellicciotti et al., 2005; Heynen et al., 2013). Additionally, the glacier module will be extended with a parameterization for modeling glacier dynamics, which would enable quantifying the retreat or advance of glaciers as a result of climate perturbations.

When SPHY is run at a spatial resolution of 1 km or coarser for mountainous regions, improvement of the respresentation of sub-grid processes becomes useful. For example, when the daily average air temperature for a given 1 km grid cell is 0 °C, no melt will be simulated for that grid cell, although the subgrid variability in elevation shows that part of the grid cell is lower than the average elevation of the grid cell and thus has temperatures above 0 °C, resulting in the generation of melt water.

Although the model is relatively easy to understand and applicable by hydrologists and scientists with basic skills, it would even be better if the model could be used by a wider group of users with basic hydrological and computer skills. Therefore, the objective of an ongoing project is to develop a Graphical User Interface (GUI) for the SPHY model. This GUI will be developed as plugin for the open-source QGIS environment, making it easy setup the model and analyse model input and output spatially and temporally.

5   Conclusions

In response to the diversity of water-related challenges, hydrologists have been developing tools to analyze, understand and explore solutions to support decision makers and operational water managers. Although progress has been made, hydrologists have put a strong emphasis on streamflow analysis and forecasting, while ignoring other hydrological processes. It is clear that not only rainfall–runoff processes are relevant, but that an integrated approach where processes as glacier and snowmelt, evapotranspiration, reservoirs, changes in landcover and landuse should be integrated in our models.

The objective of this paper is to introduce and present the SPHY model, its development background, and demonstrate some typical applications. Compared to other hydrological models, that typically focus on the simulation of streamflow only, the SPHY model has several advantages: it (i) integrates most relevant hydrological processes, (ii) is setup modular, (iii) is easy adjustable and applicable, (iii) can easily be linked to remote sensing data, and (iv) can be applied for operational as well as strategic decision support.

The most relevant hydrological processes that are integrated in the SPHY model are rainfall–runoff processes, cryosphere processes, evapotranspiration processes, the simulation of dynamic vegetational cover, lake/reservoir outflow, and the simulation of rootzone moisture contents. The capability of SPHY to successfully simulate rainfall–runoff and cryosphere processes was proven during its applications in the snow and glacier-fed river basins in Asia, and in Chile, where it was used to forecast streamflow during the snow melting season. Both the applications in Chile and in Romania show the strength of SPHY to include remotely sensed data as dynamic model input: in Chile remotely sensed snow cover was used to implement a time-variable fractional snow coverage, and in Romania the NDVI was used to simulate dynamic vegetational cover. Whereas the application in the glacier-fed river basins in Asia to study the effects of climate change on the available water resources is a typical example of the use of SPHY to support strategic decision makers, the application in Romania for real-time irrigation support, and the application in Chile to support hydropower companies for their reservoir management, are typical examples of the use of SPHY for operational purposes. The application of real-time irrigation support in Romania emphasizes the strength of SPHY to succesfully simulate other hydrological processes than rainfall–runoff as well, being evapotranspiration and rootzone soil moisture simulations. The different spatial resolutions and orograhically and climatologically regions in which SPHY was applied, demonstrate its flexibility in scaling and applicability: in Romania it was applied at the farm-field level, requiring a spatial resolution of 30 m, whereas in Chile and Asia it was applied at resolutions varying from 200 m to 1 km.

Back | Close

Full Screen / Esc

Printer-friendly Version

Interactive Discussion

The modular setup of SPHY enables it to be applied over a broad range of orographically and climatologically conditions as demonstrated in this paper: the agricultural focus in Romania allowed switching off the glaciers, snow, and routing modules, whereas these modules were switched on for the Asian and Chilean applications. Decreased model run-time, and minimzed input data requirements were the resulting benefits in cases where modules are switched off.

In summary, it can be concluded that the SPHY model is a suitable tool to be used for strategic decision as well as for operational support, having the flexibility to be applied at different spatial scales, and including the use of remote sensing data and hydrological proceses that are relevant for the area of application.

Code availability

The SPHY model is available as executable (sphy.exe) and as source code, where the source code consists of the following files:

- sphy_config.cfg
- sphy.py
- hargreaves.py
- dynamic_veg.py
- snow.py
- rootzone.py
- ET.py
- subzone.py
- glacier.py

SPHY v2.0: Spatial Processes in HYdrology

W. Terink et al.

– groundwater.py

– routing.py

– reservoir_routing.py

– reporting.py

5   – timecalc.py

The order in which the model algorithms are executed are defined in the sphy.py file, in which the required modules are imported depending on the settings in sphy_config.cfg. Model settings (parameters, input and output) can be modified in the sphy_config.cfg configuration file. It is mandatory to have this file and the source code
10 (or model executable) in the same folder on the pc's harddrive. If the user opts to run the SPHY model using the model's source code, then the SPHY model is executed by entering "python.exe sphy.py" in the windows command prompt. Otherwise, the model can be executed by entering "sphy.exe" in the windows command prompt. Both the model source code and it's executable can be obtained from the SPHY model website
15 (http://www.sphy.nl).

In order to run the SPHY model v2.0, it is required to have the following software installed on your pc:

– Python 2.7.6 (32 bit)

– NumPy 1.8.0 (32 bit)

20   – PCRaster 4.0 (32 bit)

References

ADB: Consultant's Report Regional Technical Assistance: Water and Adaptation Interventions in Central and West Asia, Tech. rep., Helsinki, Finland, 2012. 1718

Allen, R. G., Pereira, L. S., Raes, D., and Smith, M.: Crop evapotranspiration – Guidelines for computing crop water requirements, FAO Irrigation Drainage paper, Rome, Italy, 56, 1998. 1694, 1695, 1696, 1698, 1721

Bartholomeus, R. P., Witte, J.-P. M., van Bodegom, P. M., van Dam, J. C., and Aerts, R.: Critical soil conditions for oxygen stress to plant roots: substituting the Feddes-function by a process-based model, J. Hydrol., 360, 147–165, doi:10.1016/j.jhydrol.2008.07.029, 2008. 1705

Bastiaanssen, W., Allen, R., Droogers, P., D'Urso, G., and Steduto, P.: Twenty-five years modeling irrigated and drained soils: state of the art, Agr. Water Manage., 92, 111–125, doi:10.1016/j.agwat.2007.05.013, 2007. 1689

Batjes, N., Dijkshoorn, K., van Engelen, V., Fischer, G., Jones, A., Montanarella, L., Petri, M., Prieler, S., Teixeira, E., Wiberg, D., and Shi, X.: Harmonized World Soil Database (version 1.1), Tech. rep., FAO and IIASA, Rome, Italy and Laxenburg, Austria, 2009. 1720

Batjes, N., Dijkshoorn, K., van Engelen, V., Fischer, G., Jones, A., Montanarella, L., Petri, M., Prieler, S., Teixeira, E., Wiberg, D., and Shi, X.: Harmonized World Soil Database (version 1.2), Tech. rep., FAO and IIASA, Rome, Italy and Laxenburg, Austria, 2012. 1716

Bell, A., Zhu, T., Xie, H., and Ringler, C.: Climate–water interactions – challenges for improved representation in integrated assessment models, Energ. Econ., 46, 510–521, doi:10.1016/j.eneco.2013.12.016, 2014. 1690

Beven, K.: Kinematic subsurface stormflow, Water Resour. Res., 17, 1419–1424, doi:10.1029/WR017i005p01419, 1981. 1707

Beven, K.: Robert E. Horton's perceptual model of infiltration processes, Hydrol. Process., 18, 3447–3460, doi:10.1002/hyp.5740, 2004. 1706

Beven, K. and Germann, P.: Macropores and water flow in soils, Water Resour. Res., 18, 1311–1325, doi:10.1029/WR018i005p01311, 1982. 1707

Biswas, A. K. and Tortajada, C.: Future water governance: problems and perspectives, Int. J. Water Resour. D., 26, 129–139, doi:10.1080/07900627.2010.488853, 2010. 1688

Bontemps, S., Defourny, P., van Bogaert, E., Arino, O., Kalogirou, V., and Ramos Perez, J.: GLOBCOVER 2009. Products Description and Validation Report, Tech. rep., ESA, Louvain, Belgium, 2011. 1720

Title Page

Abstract | Introduction

Conclusions | References

Tables | Figures

◀ | ▶

◀ | ▶

Back | Close

Full Screen / Esc

Printer-friendly Version

Interactive Discussion

Bowling, L. C., Pomeroy, J. W., and Lettenmaier, D. P.: Parameterization of Blowing-Snow Sublimation in a Macroscale Hydrology Model, J. Hydrometeorol., 5, 745–762, doi:10.1175/1525-7541(2004)005<0745:POBSIA>2.0.CO;2, 2004. 1723

Bramer, L. M., Hornbuckle, B. K., and Caragea, P. C.: How many measurements of soil moisture within the footprint of a ground-based microwave radiometer are required to account for meter-scale spatial variability?, Vadose Zone J., 12, 3, doi:10.2136/vzj2012.0100, 2013. 1717

Brutsaert, W.: De Saint-Venant equations experimentally verified, J. Hydr. Eng. Div.-ASCE, 97, 1387–1401, 1971. 1712

Brutsaert, W.: Hydrology. An Introduction, Cambridge University Press, Cambridge, 2005. 1723

Carlson, T. N. and Ripley, D. A.: On the relation between NDVI, fractional vegetation cover, and leaf area index, Remote Sens. Environ., 62, 241–252, doi:10.1016/S0034-4257(97)00104-1, 1997. 1692, 1696

Corradini, C., Morbidelli, R., and Melone, F.: On the interaction between infiltration and Hortonian runoff, J. Hydrol., 204, 52–67, doi:10.1016/S0022-1694(97)00100-5, 1998. 1706

Dai, A.: Drought under global warming: a review, Wiley Interdisciplinary Reviews: Climate Change, 2, 45–65, doi:10.1002/wcc.81, 2011. 1689

de Jong, S. and Jetten, V.: Distributed, quantitative assessment of canopy storage capacity by Hyperspectral Remote Sensing, available at: http://www.geo.uu.nl/dejong/pdf-files/Interception-by-RS.pdf (last access: 13 November 2014), 2010. 1697

Droogers, P. and Aerts, J.: Adaptation strategies to climate change and climate variability: a comparative study between seven contrasting river basins, Phys. Chem. Earth Pt. A/B/C, 30, 339–346, doi:10.1016/j.pce.2005.06.015, 2005. 1689

Droogers, P. and Allen, R. G.: Estimating reference evapotranspiration under inaccurate data conditions, Irrig. Drain. Syst., 16, 33–45, doi:10.1023/A:1015508322413, 2002. 1694

Droogers, P. and Bouma, J.: Simulation modelling for water governance in basins, Int. J. Water Resour. D., 30, 1–20, doi:10.1080/07900627.2014.903771, 2014. 1688, 1689

Droogers, P. and Immerzeel, W. W.: Wat is het beste model?, H2O Tijdschrift voor watervoorziening en waterbeheer, 4, 38–41, 2010. 1691

Droogers, P. and Kite, G.: Remotely sensed data used for modelling at different hydrological scales, Hydrol. Process., 16, 1543–1556, doi:10.1002/hyp.1019, 2002. 1690

Title Page

Abstract | Introduction

Conclusions | References

Tables | Figures

|◄ | ►|

◄ | ►

Back | Close

Full Screen / Esc

Printer-friendly Version

Interactive Discussion

Droogers, P., Immerzeel, W. W., Terink, W., Hoogeveen, J., Bierkens, M. F. P., van Beek, L. P. H., and Debele, B.: Water resources trends in Middle East and North Africa towards 2050, Hydrol. Earth Syst. Sci., 16, 3101–3114, doi:10.5194/hess-16-3101-2012, 2012. 1689

EEA: EU-DEM layers, Copernicus data and information funded by the European Union, European Environmental Agency, Tech. rep., Copenhague, Denmark, 2014. 1716

EPA: Modeling at EPA, available at: http://www.epa.gov/epahome/models.htm (last access: 30 September 2014), 2014. 1689

Falkenmark, M. and Rockström, J.: Building water resilience in the face of global change: from a blue-only to a green-blue water approach to land-water management, J. Water Res. Pl.-ASCE, 136, 606–610, doi:10.1061/(ASCE)WR.1943-5452.0000118, 2010. 1690

Feddes, R., Kowalik, P., and Zaradny, H.: Simulation of field water use and crop yield. Simulation Monographs, Wageningen University, Pudoc, 1978. 1706

Foglia, L., Hill, M. C., Mehl, S. W., and Burlando, P.: Sensitivity analysis, calibration, and testing of a distributed hydrological model using error-based weighting and one objective function, Water Resour. Res., 45, 6, doi:10.1029/2008WR007255, 2009. 1717

Gat, J. R., Bowser, C. J., and Kendall, C.: The contribution of evaporation from the Great Lakes to the continental atmosphere: estimate based on stable isotope data, Geophys. Res. Lett., 21, 557–560, doi:10.1029/94GL00069, 1994. 1722

Gill, M. A.: Flood routing by the Muskingum method, J. Hydrol., 36, 353–363, doi:10.1016/0022-1694(78)90153-1, 1978. 1713, 1723

Gopalan, K., Wang, N.-Y., Ferraro, R., and Liu, C.: Status of the TRMM 2A12 Land Precipitation Algorithm, J. Atmos. Ocean. Tech., 27, 1343–1354, doi:10.1175/2010JTECHA1454.1, 2010. 1718

Goward, S. N. and Huemmrich, K. F.: Vegetation canopy PAR absorptance and the normalized difference vegetation index: an assessment using the SAIL model, Remote Sens. Environ., 39, 119–140, doi:10.1016/0034-4257(92)90131-3, 1992. 1697

Groot Zwaaftink, C. D., Mott, R., and Lehning, M.: Seasonal simulation of drifting snow sublimation in Alpine terrain, Water Resour. Res., 49, 1581–1590, doi:10.1002/wrcr.20137, 2013. 1723

Hall, D. K., Riggs, G. A., Salomonson, V. V., DiGirolamo, N. E., and Bayr, K. J.: MODIS snow-cover products, Remote Sens. Environ., 83, 181–194, doi:10.1016/S0034-4257(02)00095-0, 2002. 1719

Harbaugh, A., Banta, E., Hill, M., and McDonald, M.: MODFLOW-2000, the U.S. Geological survey modular ground-water model – user guide to modularization concepts and the ground-water flow process, US Geological Survey Reston, Virginia, 2000. 1689

Hargreaves, G. H. and Samani, Z. A.: Reference crop evapotranspiration from temperature, Appl. Eng. Agric., 1, 96–99, doi:10.13031/2013.26773, 1985. 1694, 1721

HEC: Hydrologic Engineering Center (HEC) computer software for hydrologic engineering and planning analysis, available at: http://www.hec.usace.army.mil/software/ (last access: 3 September 2014), 2014. 1689

Hewlett, J.: Soil moisture as a source of base flow from steep mountain watershed, Tech. rep., US Forest Service, Southeastern Forest Experiment Station, Asheville, North Carolina, 1961. 1706

Heynen, M., Pellicciotti, F., and Carenzo, M.: Parameter sensitivity of a distributed enhanced temperature-index melt model, Ann. Glaciol., 54, 311–321, doi:10.3189/2013AoG63A537, 2013. 1724

Hijmans, R. J., Cameron, S. E., Parra, J. L., Jones, P. G., and Jarvis, A.: Very high resolution interpolated climate surfaces for global land areas, Int. J. Climatol., 25, 1965–1978, doi:10.1002/joc.1276, 2005. 1720

Hock, R.: Temperature index melt modelling in mountain areas, J. Hydrol., 282, 104–115, doi:10.1016/S0022-1694(03)00257-9, 2003. 1700, 1724

Hock, R.: Glacier melt: a review of processes and their modelling, Prog. Phys. Geog., 29, 362–391, doi:10.1191/0309133305pp453ra, 2005. 1700, 1702

Hooghoudt, S.: Bijdragen tot de kennis van eenige natuurkundige grootheden van den grond. No. 7. Algemeene beschouwing van het probleem van de detailontwatering en de infiltratie door middel van parallel loopende drains, greppels, slooten en kanalen, Versl. Landbouwkd. Onderz., 46, 515–707, 1940. 1710

Hunink, J., Niadas, I., Antonaropoulos, P., Droogers, P., and de Vente, J.: Targeting of intervention areas to reduce reservoir sedimentation in the Tana catchment (Kenya) using SWAT, Hydrolog. Sci. J., 58, 600–614, doi:10.1080/02626667.2013.774090, 2013. 1722

Immerzeel, W. W. and Droogers, P.: Calibration of a distributed hydrological model based on satellite evapotranspiration, J. Hydrol., 349, 411–424, doi:10.1016/j.jhydrol.2007.11.017, 2008. 1717

Immerzeel, W. W. and Bierkens, M. F. P.: Asia's water balance, Nat. Geosci., 5, 841–842, doi:10.1038/ngeo1643, 2012. 1718

Immerzeel, W. W., van Beek, L. P. H., and Bierkens, M. F. P.: Climate change will affect the Asian water towers, Science, 328, 1382–1385, doi:10.1126/science.1183188, 2010. 1718

Immerzeel, W. W., Beek, L. P. H., Konz, M., Shrestha, A. B., and Bierkens, M. F. P.: Hydrological response to climate change in a glacierized catchment in the Himalayas, Climatic Change, 110, 721–736, doi:10.1007/s10584-011-0143-4, 2011. 1689, 1691

Ines, A. V., Honda, K., Das Gupta, A., Droogers, P., and Clemente, R. S.: Combining remote sensing-simulation modeling and genetic algorithm optimization to explore water management options in irrigated agriculture, Agr. Water Manage., 83, 221–232, doi:10.1016/j.agwat.2005.12.006, 2006. 1690

Irrisoft: Database and on-line Applications in Irrigation, Drainage & Hydrology, available at: http://www.irrisoft.org (last access: 7 May 2014), 2014. 1689

Karssenberg, D.: The value of environmental modelling languages for building distributed hydrological models, Hydrol. Process., 16, 2751–2766, doi:10.1002/hyp.1068, 2002. 1691

Karssenberg, D., Burrough, P. A., Sluiter, R., and de Jong, K.: The PCRaster software and course materials for teaching numerical modelling in the environmental sciences, Transactions in GIS, 5, 99–110, doi:10.1111/1467-9671.00070, 2001. 1691

Karssenberg, D., Schmitz, O., Salamon, P., de Jong, K., and Bierkens, M. F.: A software framework for construction of process-based stochastic spatio-temporal models and data assimilation, Environ. Modell. Softw., 25, 489–502, doi:10.1016/j.envsoft.2009.10.004, 2010. 1691

Kauffman, S., Droogers, P., Hunink, J., Mwaniki, B., Muchena, F., Gicheru, P., Bindraban, P., Onduru, D., Cleveringa, R., and Bouma, J.: Green Water Credits – exploring its potential to enhance ecosystem services by reducing soil erosion in the Upper Tana basin, Kenya, Int. J. Biodiversity Science, Ecosystem Services & Management, 10, 133–143, doi:10.1080/21513732.2014.890670, 2014. 1722

Khakbaz, B., Imam, B., Hsu, K., and Sorooshian, S.: From lumped to distributed via semi-distributed: calibration strategies for semi-distributed hydrologic models, J. Hydrol., 418–419, 61–77, doi:10.1016/j.jhydrol.2009.02.021, 2012. 1690

Kite, G. and Droogers, P.: Comparing evapotranspiration estimates from satellites, hydrological models and field data, J. Hydrol., 229, 1–2, 2000. 1690

Kokkonen, T., Koivusalo, H., Jakeman, A., and Norton, J.: Construction of a Degree-Day Snow Model in the Light of the "Ten Iterative Steps in Model Development", in: Proceedings of the iEMSs Third Biennial Meeting: Summit on Environmental Modelling Software, Environmental

Title Page

Abstract | Introduction

Conclusions | References

Tables | Figures

|◄ | ►|

◄ | ►

Back | Close

Full Screen / Esc

Printer-friendly Version

Interactive Discussion

Modelling Software Society, Burlington, USA, available at: http://www.iemss.org/iemss2006/papers/w4/Kokkonen.pdf, 2006. 1699

Kozak, J. A., Ahuja, L. R., Green, T. R., and Ma, L.: Modelling crop canopy and residue rainfall interception effects on soil hydrological components for semi-arid agriculture, Hydrol. Process., 21, 229–241, doi:10.1002/hyp.6235, 2007. 1697

Lambert, J., Daroussin, J., Eimberck, M., Le Bas, C., Jamagne, M., King, D., and Montanarella, L.: Soil Geographical Database for Eurasia & The Mediterranean. Instructions Guide for Elaboration at scale 1 : 1,000,000 version 4.0. EUR 20422 EN, Tech. rep., JRC, Ispra, Italy, 2003. 1716

Lenaerts, J. T. M., van den Broeke, M. R., Déry, S. J., König-Langlo, G., Ettema, J., and Munneke, P. K.: Modelling snowdrift sublimation on an Antarctic ice shelf, The Cryosphere, 4, 179-190, doi:10.5194/tc-4-179-2010, 2010. 1723

Liu, Y., Gupta, H., Springer, E., and Wagener, T.: Linking science with environmental decision making: experiences from an integrated modeling approach to supporting sustainable water resources management, Environ. Modell. Softw., 23, 846–858, doi:10.1016/j.envsoft.2007.10.007, 2008. 1689, 1690

Lutz, A., Droogers, P., and Immerzeel, W.: Climate Change Impact and Adaptation on the Water Resources in the Amu Darya and Syr Darya River Basins, Tech. rep., FutureWater, Wageningen, 2012a. 1717, 1718

Lutz, A. F., Immerzeel, W. W., and Droogers, P.: Climate Change Impacts on the Upstream Water Resources of the Amu and Syr Darya River Basins, Tech. rep., FutureWater report 107, Wageningen, 2012b. 1717, 1718

Lutz, A. F., Immerzeel, W. W., Gobiet, A., Pellicciotti, F., and Bierkens, M. F. P.: Comparison of climate change signals in CMIP3 and CMIP5 multi-model ensembles and implications for Central Asian glaciers, Hydrol. Earth Syst. Sci., 17, 3661–3677, doi:10.5194/hess-17-3661-2013, 2013. 1719

Lutz, A. F., Immerzeel, W. W., Shrestha, A. B., and Bierkens, M. F. P.: Consistent increase in High Asia's runoff due to increasing glacier melt and precipitation, Nature Climate Change, 4, 587–592, doi:10.1038/nclimate2237, 2014. 1717, 1719, 1744, 1745

MacDonald, M. K., Pomeroy, J. W., and Pietroniro, A.: Parameterizing redistribution and sublimation of blowing snow for hydrological models: tests in a mountainous subarctic catchment, Hydrol. Process., 23, 2570–2583, doi:10.1002/hyp.7356, 2009. 1723

Title Page

Abstract | Introduction

Conclusions | References

Tables | Figures

◀ | ▶

◀ | ▶

Back | Close

Full Screen / Esc

Printer-friendly Version

Interactive Discussion

Manning, R.: On the flow of water in open channels and pipes, Trans. Inst. Civ. Eng. Ireland, 20, 161–207, 1989. 1713

Meehl, G. A., Covey, C., Taylor, K. E., Delworth, T., Stouffer, R. J., Latif, M., McAvaney, B., and Mitchell, J. F. B.: THE WCRP CMIP3 multimodel dataset: a new era in climate change research, B. Am. Meteorol. Soc., 88, 1383–1394, doi:10.1175/BAMS-88-9-1383, 2007. 1718

Moreda, F., Koren, V., Zhang, Z., Reed, S., and Smith, M.: Parameterization of distributed hydrological models: learning from the experiences of lumped modeling, J. Hydrol., 320, 218–237, doi:10.1016/j.jhydrol.2005.07.014, 2006. 1690

Morris, E. M. and Woolhiser, D. A.: Unsteady one-dimensional flow over a plane: partial equilibrium and recession hydrographs, Water Resour. Res., 16, 355–360, doi:10.1029/WR016i002p00355, 1980. 1712

Myneni, R. and Williams, D.: On the relationship between FAPAR and NDVI, Remote Sens. Environ., 49, 200–211, doi:10.1016/0034-4257(94)90016-7, 1994. 1692

Nash, J. and Sutcliffe, J.: River flow forecasting through conceptual models part I – A discussion of principles, J. Hydrol., 10, 282–290, doi:10.1016/0022-1694(70)90255-6, 1970. 1717, 1720

Neitsch, S. L., Arnold, J. G., Kiniry, J. R., and Williams, J. R.: Soil and Water Assessment Tool (SWAT). Theoretical Documentation, version 2009, Tech. rep., Texas Water Resources Institute, College Station, Texas, available at: http://twri.tamu.edu/reports/2011/tr406.pdf (last access: 4 June 2014), 2009. 1690, 1691, 1708, 1709, 1710, 1711, 1713

Parajka, J. and Blöschl, G.: Spatio-temporal combination of MODIS images – potential for snow cover mapping, Water Resour. Res., 44, 3, doi:10.1029/2007WR006204, 2008. 1719

Park, C. C.: World-wide variations in hydraulic geometry exponents of stream channels: an analysis and some observations, J. Hydrol., 33, 133–146, doi:10.1016/0022-1694(77)90103-2, 1977. 1723

Pellicciotti, F., Brock, B., Strasser, U., Burlando, P., Funk, M., and Corripio, J.: An enhanced temperature-index glacier melt model including the shortwave radiation balance: development and testing for Haut Glacier d'Arolla, Switzerland, J. Glaciol., 51, 573–587, doi:10.3189/172756505781829124, 2005. 1724

Peng, D., Zhang, B., and Liu, L.: Comparing spatiotemporal patterns in Eurasian FPAR derived from two NDVI-based methods, Int. J. Digital Earth, 5, 283–298, doi:10.1080/17538947.2011.598193, 2012. 1696

Rafn, E. B., Contor, B., and Ames, D. P.: Evaluation of a method for estimating irrigated crop–evapotranspiration coefficients from remotely sensed data in Idaho, J. Irrig. Drain. E.-ASCE, 134, 722–729, doi:10.1061/(ASCE)0733-9437(2008)134:6(722), 2008. 1695

Reid, T. D., Carenzo, M., Pellicciotti, F., and Brock, B. W.: Including debris cover effects in a distributed model of glacier ablation, J. Geophys. Res., 117, D18, doi:10.1029/2012JD017795, 2012. 1702

Rockström, J., Falkenmark, M., Lannerstad, M., and Karlberg, L.: The planetary water drama: dual task of feeding humanity and curbing climate change, Geophys. Res. Lett., 39, 15, doi:10.1029/2012GL051688, 2012. 1689

Rollenbeck, R. and Bendix, J.: Rainfall distribution in the Andes of southern Ecuador derived from blending weather radar data and meteorological field observations, Atmos. Res., 99, 277–289, doi:10.1016/j.atmosres.2010.10.018, 2011. 1720, 1721

Samain, B., Simons, G. W. H., Voogt, M. P., Defloor, W., Bink, N.-J., and Pauwels, V. R. N.: Consistency between hydrological model, large aperture scintillometer and remote sensing based evapotranspiration estimates for a heterogeneous catchment, Hydrol. Earth Syst. Sci., 16, 2095–2107, doi:10.5194/hess-16-2095-2012, 2012. 1717

Sangrey, D. A., Harrop-Williams, K. O., and Klaiber, J. A.: Predicting Ground-Water Response to Precipitation, J. Geotech. Eng-ASCE, 110, 957–975, doi:10.1061/(ASCE)0733-9410(1984)110:7(957), 1984. 1710

Schaner, N., Voisin, N., Nijssen, B., and Lettenmaier, D. P.: The contribution of glacier melt to streamflow, Environ. Res. Lett., 7, 034029, doi:10.1088/1748-9326/7/3/034029, 2012. 1718

Schmitz, O., Karssenberg, D., van Deursen, W., and Wesseling, C.: Linking external components to a spatio-temporal modelling framework: coupling MODFLOW and PCRaster, Environ. Modell. Softw., 24, 1088–1099, doi:10.1016/j.envsoft.2009.02.018, 2009. 1691

Schmitz, O., Karssenberg, D., de Jong, K., de Kok, J.-L., and de Jong, S. M.: Map algebra and model algebra for integrated model building, Environ. Modell. Softw., 48, 113–128, doi:10.1016/j.envsoft.2013.06.009, 2013. 1691

Sellers, P. J., Tucker, C. J., Collatz, G. J., Los, S. O., Justice, C. O., Dazlich, D. A., and Randall, D. A.: A revised land surface parameterization (SiB2) for atmospheric GCMS. Part II: The generation of global fields of terrestrial biophysical parameters from satellite data, J. Climate, 9, 706–737, doi:10.1175/1520-0442(1996)009<0706:ARLSPF>2.0.CO;2, 1996. 1696, 1739

Sheffield, J., Goteti, G., and Wood, E. F.: Development of a 50-year high-resolution global dataset of meteorological forcings for land surface modeling, J. Climate, 19, 3088–3111, doi:10.1175/JCLI3790.1, 2006. 1718

Singh, P. and Kumar, N.: Impact assessment of climate change on the hydrological response of a snow and glacier melt runoff dominated Himalayan river, J. Hydrol., 193, 316–350, doi:10.1016/S0022-1694(96)03142-3, 1997. 1693

Sloan, P. G. and Moore, I. D.: Modeling subsurface stormflow on steeply sloping forested watersheds, Water Resour. Res., 20, 1815–1822, doi:10.1029/WR020i012p01815, 1984. 1707, 1708

Smedema, L. and Rycroft, D.: Land Drainage: Planning and Design of Agricultural Drainage Systems, Cornell University Press, Ithaca, New York, USA, 1983. 1710

Smith, M. B., Seo, D.-J., Koren, V. I., Reed, S. M., Zhang, Z., Duan, Q., Moreda, F., and Cong, S.: The distributed model intercomparison project (DMIP): motivation and experiment design, J. Hydrol., 298, 4–26, doi:10.1016/j.jhydrol.2004.03.040, 2004. 1690

Smith, M. B., Koren, V., Reed, S., Zhang, Z., Zhang, Y., Moreda, F., Cui, Z., Mizukami, N., Anderson, E. A., and Cosgrove, B. A.: The distributed model intercomparison project – Phase 2: Motivation and design of the Oklahoma experiments, J. Hydrol., 418–419, 3–16, doi:10.1016/j.jhydrol.2011.08.055, 2012. 1690

Sorg, A., Bolch, T., Stoffel, M., Solomina, O., and Beniston, M.: Climate change impacts on glaciers and runoff in Tien Shan (Central Asia), Nature Climate Change, 2, 725–731, doi:10.1038/nclimate1592, 2012. 1718

Sperna Weiland, F. C., van Beek, L. P. H., Kwadijk, J. C. J., and Bierkens, M. F. P.: Global patterns of change in discharge regimes for 2100, Hydrol. Earth Syst. Sci., 16, 1047–1062, doi:10.5194/hess-16-1047-2012, 2012. 1691

Strasser, U., Bernhardt, M., Weber, M., Liston, G. E., and Mauser, W.: Is snow sublimation important in the alpine water balance?, The Cryosphere, 2, 53–66, doi:10.5194/tc-2-53-2008, 2008. 1723

Taylor, K. E., Stouffer, R. J., and Meehl, G. A.: An Overview of CMIP5 and the Experiment Design, B. Am. Meteorol. Soc., 93, 485–498, doi:10.1175/BAMS-D-11-00094.1, 2012. 1718

Tucker, C. J.: Red and photographic infrared linear combinations for monitoring vegetation, Remote Sens. Environ., 8, 127–150, doi:10.1016/0034-4257(79)90013-0, 1979. 1692

USGS: Landsat 8: U.S. Geological Survey Fact Sheet 2013–3060, Tech. rep., available at: http://pubs.usgs.gov/fs/2013/3060/ (last access: 15 June 2014), 2013. 1716

USGS: Water Resources Applications Software, available at: http://water.usgs.gov/software/lists/alphabetical (last access: 30 April 2014), 2014. 1689

van Dam, J. C., Huygen, J., Wesseling, J. G., Feddes, R. A., Kabat, P., van Walsum, P. E. V., Groenendijk, P., and van Diepen., C. A.: Theory of SWAP version 2.0. Simulation of water flow, solute transport and plant growth in the Soil–Water–Atmosphere–Plant environment, Tech. rep., Department Water Resources, Wageningen Agricultural University, Wageningen, the Netherlands, 1997. 1691, 1721

Van Genuchten, M.: A closed-form equation for predicting the hydraulic conductivity of unsaturated soils, Soil Sci. Soc. Am. J., 44, 892–898, 1980. 1716

Venetis, C.: A study on the recession of unconfined acquifers, Int. Assoc. Scientific Hydrol. B., 14, 119–125, doi:10.1080/02626666909493759, 1969. 1710

Verbunt, M., Gurtz, J., Jasper, K., Lang, H., Warmerdam, P., and Zappa, M.: The hydrological role of snow and glaciers in alpine river basins and their distributed modeling, J. Hydrol., 282, 36–55, doi:10.1016/S0022-1694(03)00251-8, 2003. 1693

Von Hoyningen-Huene, J.: Die Interzeption des Niederschlags in landwirtschaftlichen Pflanzenbeständen, Arbeitsbericht Deutscher Verband fur Wasserwirtschaft und Kulturbau, DWK, Braunschweig, Germany, 1981. 1697

Wagner, P. D., Fiener, P., Wilken, F., Kumar, S., and Schneider, K.: Comparison and evaluation of spatial interpolation schemes for daily rainfall in data scarce regions, J. Hydrol., 464–465, 388–400, doi:10.1016/j.jhydrol.2012.07.026, 2012. 1721

Walter, I. A., Allen, R. G., Elliott, R., Jensen, M. E., Itenfisu, D., Mecham, B., Howell, T. A., Snyder, R., Brown, P., Echings, S., Spofford, T., Hattendorf, M., Cuenca, R. H., Wright, J. L., and Martin, D.: ASCE's Standardized Reference Evapotranspiration Equation, in: Watershed Management and Operations Management 2000, American Society of Civil Engineers, Reston, VA, 1–11, doi:10.1061/40499(2000)126, 2001. 1694

Wanders, N., Bierkens, M. F. P., de Jong, S. M., de Roo, A., and Karssenberg, D.: The benefits of using remotely sensed soil moisture in parameter identification of large-scale hydrological models, Water Resour. Res., 50, 6874–6891, doi:10.1002/2013WR014639, 2014. 1690

Wheeler, T. and von Braun, J.: Climate change impacts on global food security, Science, 341, 508–513, doi:10.1126/science.1239402, 2013. 1689

Williams, J.: HYMO flood routing, J. Hydrol., 26, 17–27, doi:10.1016/0022-1694(75)90122-5, 1975. 1713

Title Page

Abstract | Introduction

Conclusions | References

Tables | Figures

|◀ | ▶|

◀ | ▶

Back | Close

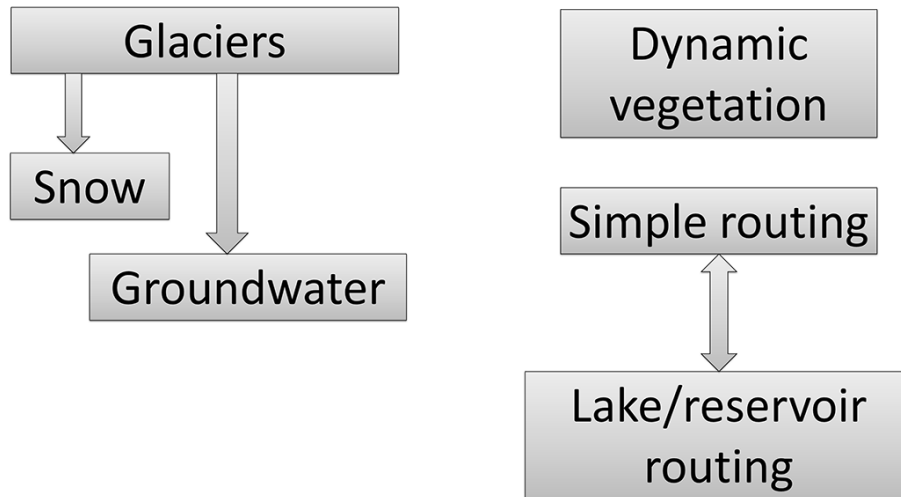Full Screen / Esc

Printer-friendly Version

Interactive Discussion

Yatagai, A., Kamiguchi, K., Arakawa, O., Hamada, A., Yasutomi, N., and Kitoh, A.: APHRODITE: constructing a long-term daily gridded precipitation dataset for asia based on a dense network of rain gauges, B. Am. Meteorol. Soc., 93, 1401–1415, doi:10.1175/BAMS-D-11-00122.1, 2012. 1718

Title Page

Abstract | Introduction

Conclusions | References

Tables | Figures

◄ | ►

◄ | ►

Back | Close

Full Screen / Esc

Printer-friendly Version

Interactive Discussion

Table 1. LAI_{max} values for different vegetation types (Sellers et al., 1996).

Vegetation type	LAI_{max} [–]
Broadleaf evergreen trees	7
Broadleaf deciduous trees	7
Mixed trees	7.5
Needleleaf evergreen trees	8
High latitude deciduous trees	8
Grass with 10–40 % woody cover	5
Grass with < 10 % woody cover	5
Shrubs and bare soil	5
Moss and lichens	5
Bare	5
Cultivated	6
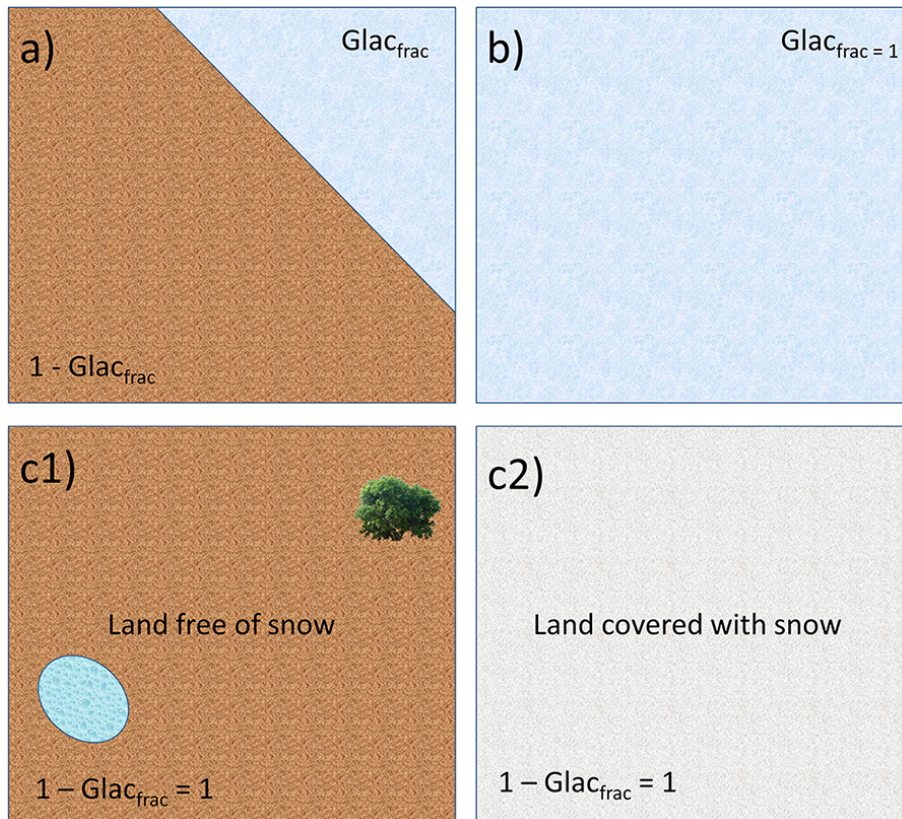
Figure 1. Illustration of SPHY sub-grid variability. A grid-cell in SPHY can be **(a)** partially covered with glaciers, or **(b)** completely covered with glaciers, or **(c1)** free of snow, or **(c2)** completely covered with snow. In case of **(c1)**, the free land surface can consist of bare soil, vegetation, or open water.

Title Page

Abstract | Introduction

Conclusions | References

Tables | Figures

|◀ | ▶|

◀ | ▶

Back | Close

Full Screen / Esc

Printer-friendly Version

Interactive Discussion
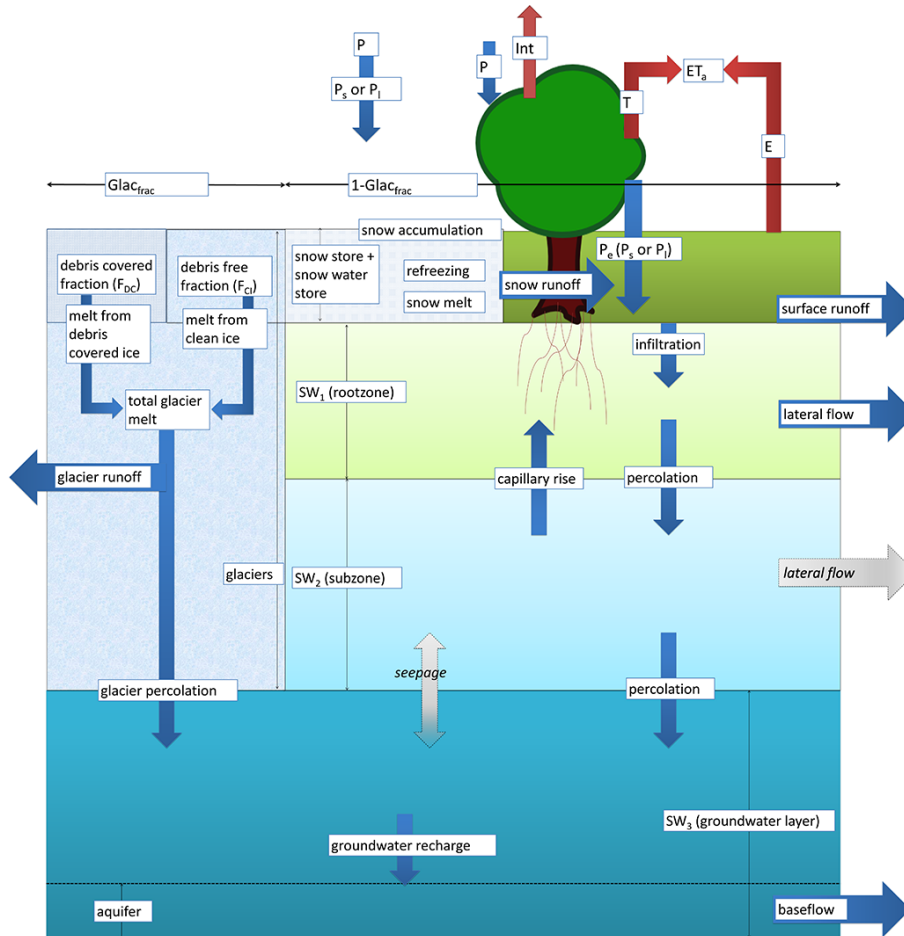
Figure 2. SPHY model concepts. The fluxes in grey are only incorporated when the groundwater module is not used. Abbreveations are explained in the text.

Figure 3. Modules of the SPHY model that can be switched on/off.
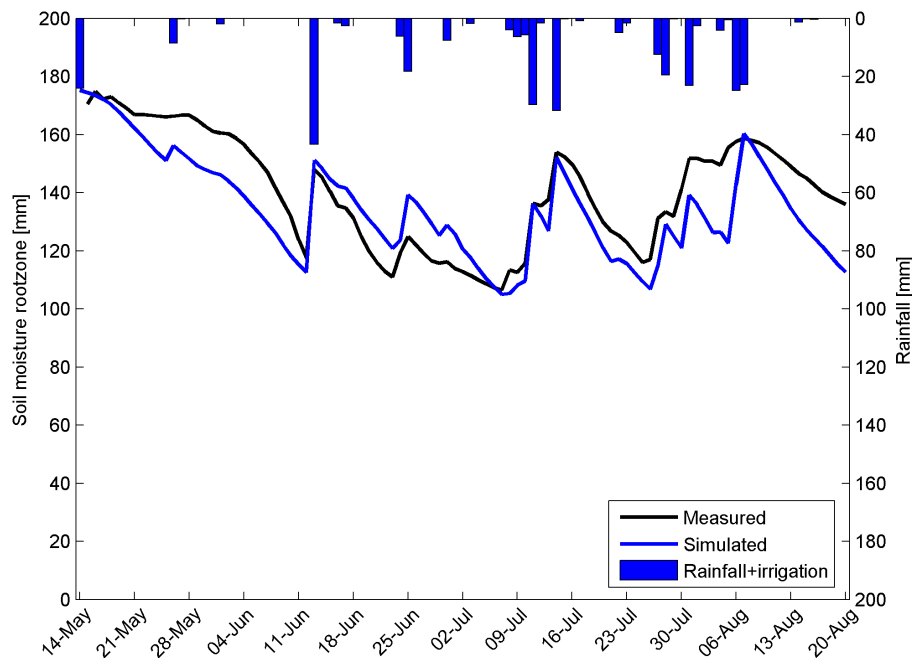
Figure 4. Measured and simulated daily rootzone soil moisture content during the 2014 growing season. Rainfall + irrigation has been measured by the rain gauge that was attached to the moisture sensor.
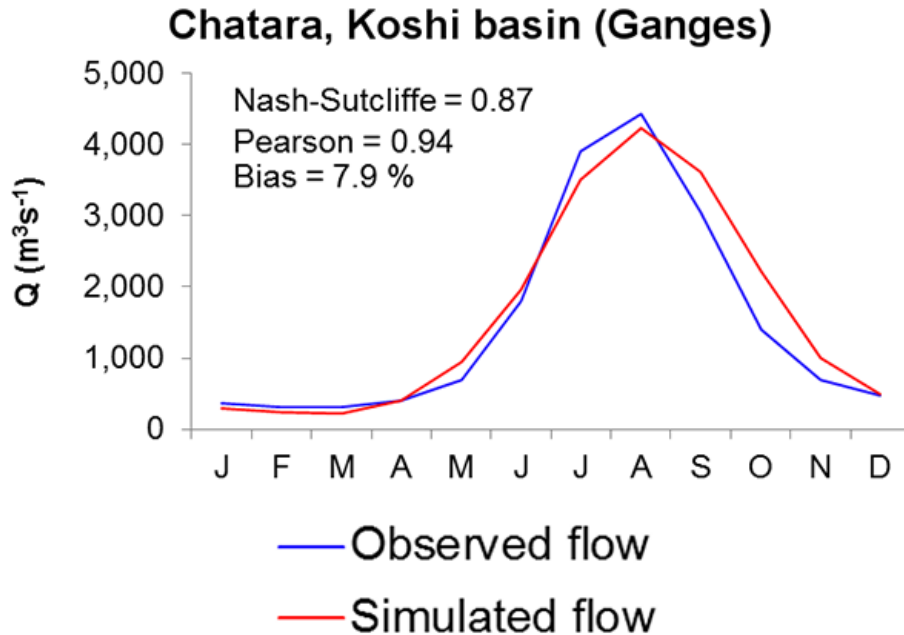
Figure 5. Average monthly observed and SPHY-simulated flow (1998–2007) for the Chatara major discharge measurment location in the Ganges basin (Lutz et al., 2014).

Figure 6. The contribution of glacier melt **(a)**, snow melt **(b)**, and rainfall **(c)** to the total flow for major streams in the upstream basins of the Indus, Ganges, Brahmaputra, Salween and Mekong during 1998–2007 (Lutz et al., 2014).

Title Page

Abstract | Introduction

Conclusions | References

Tables | Figures

◄◄ | ►►

◄ | ►

Back | Close

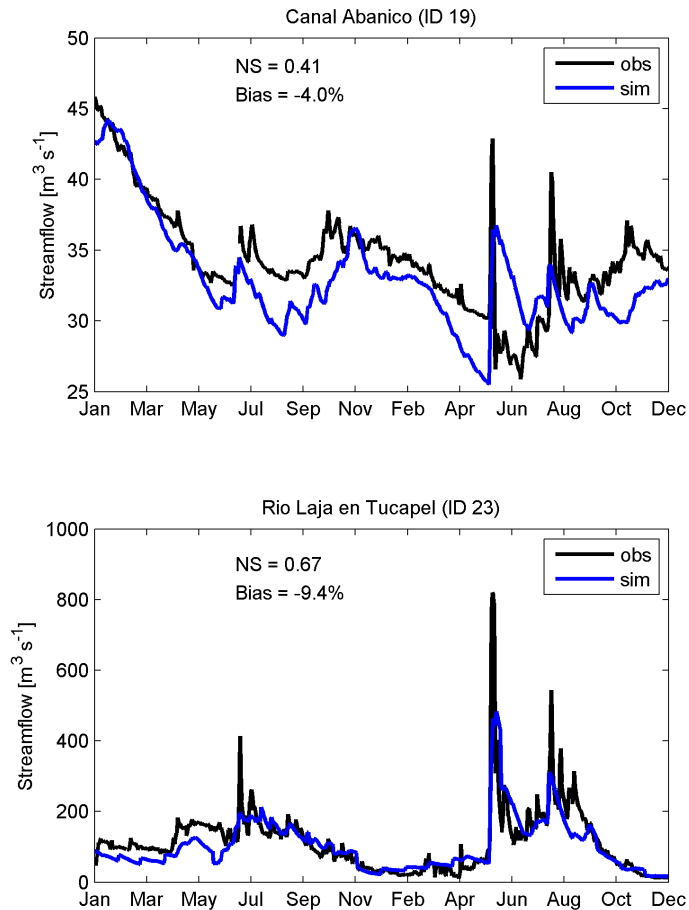Full Screen / Esc

Printer-friendly Version

Interactive Discussion
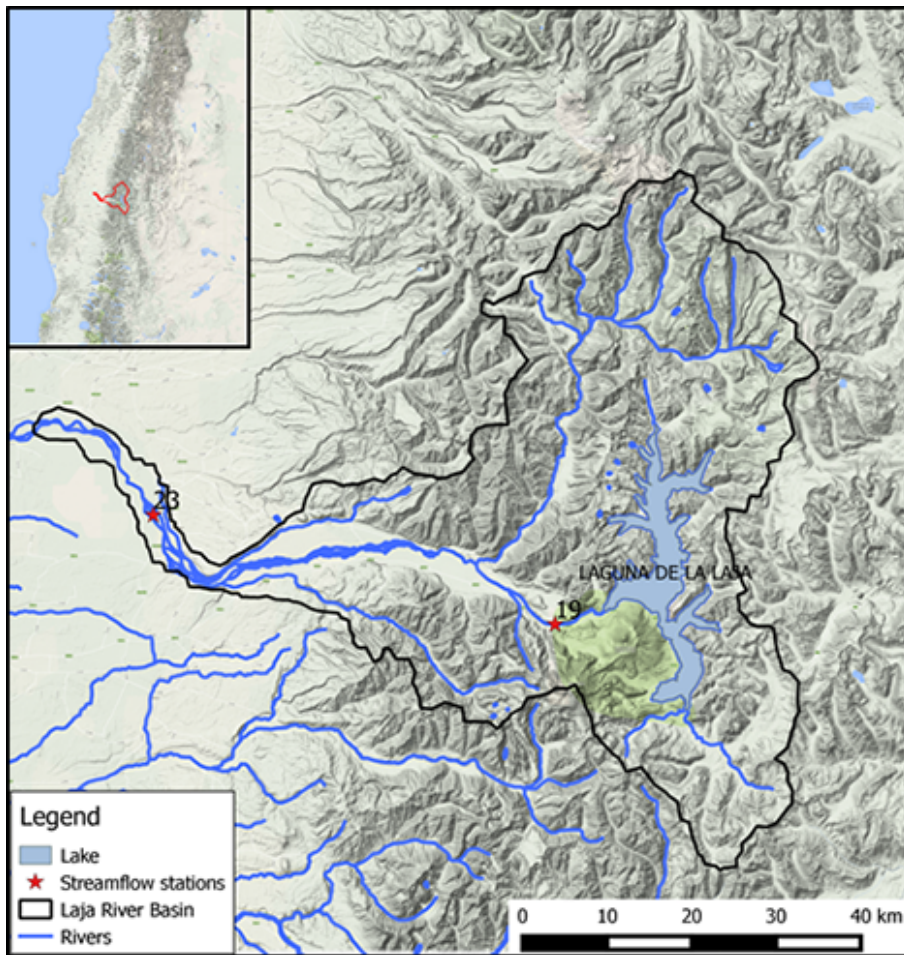
Figure 7. Laja River Basin in Chile with Laja Lake and the streamflow stations Canal Abanico (ID 19) and Rio Laja en Tucapel (ID 23).

Figure 8. Daily observed vs. SPHY simulated streamflow (period 2007–2008) for the streamflow stations Canal Abanicao (ID 19) and Rio Laja en Tucapel (ID 23). The Nash–Sutcliffe (NS) and bias model performance indicators are shown as well.

Title Page

Abstract | Introduction

Conclusions | References

Tables | Figures

|◄ | ►|

◄ | ►

Back | Close

Full Screen / Esc

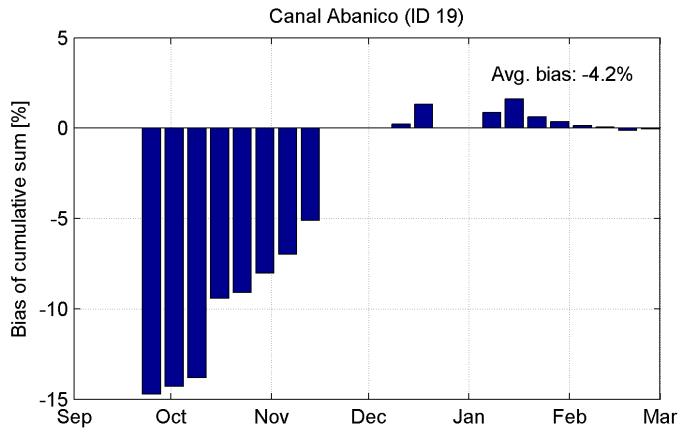Printer-friendly Version

Interactive Discussion
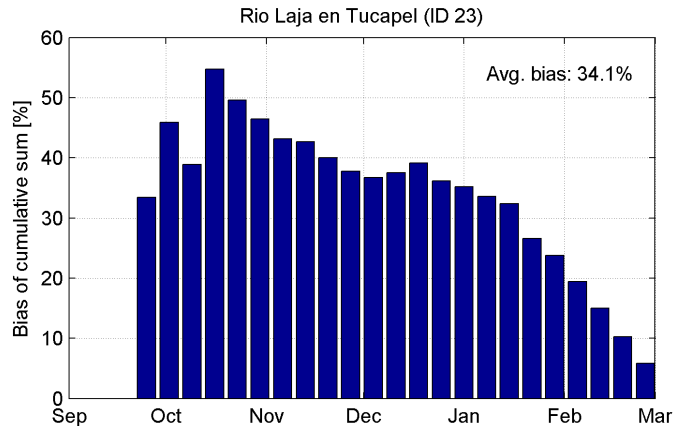
Figure 9. Bias between total cumulative forecasted flow and observed flow for the 23 model runs that were executed between the end of September 2013 and March 2014. Results are shown for the locations Canal Abanicao (ID 19) and Rio Laja en Tucapel (ID 23).